Journal of Electroanalytical Chemistry 895 (2021) 115483

Contents lists available at ScienceDirect

Journal of Electroanalytical Chemistry

journal homepage: www.elsevier.com/locate/jelechem

Effect of thiophene, 3-hexylthiophene, selenophene, and Thieno[3,2-*b*] thiophene spacers on OPV device performance of novel 2,1,3-benzothiadiazole based alternating copolymers

Cansu Zeytun Karaman [a], Seza Göker [b], Ümmügülsüm Şahin [a], Serife O. Hacioglu [c], Sultan Taşkaya Aslan [a], Tuğba Hacıefendioğlu [a], Gonul Hizalan [d,e], Erol Yıldırım [a,f,g], Ali Çırpan [a,e,f,g], Levent Toppare [a,e,g,*]

[a] *Chemistry Department, Middle East Technical University, Ankara 06800, Turkey*
[b] *Solid Propellant Department, Roketsan Missiles Inc., Ankara 06500, Turkey*
[c] *Department of Engineering Basic Sciences of Engineering, Faculty of Engineering and Natural Sciences, Iskenderun Technical University, Hatay 31200, Turkey*
[d] *ODTÜ-GÜNAM, Middle East Technical University, 06800 Ankara, Turkey*
[e] *The Center for Solar Energy Research and Application (GUNAM), Middle East Technical University, 06800 Ankara, Turkey*
[f] *Department of Micro and Nanotechnology, Middle East Technical University, 06800 Ankara, Turkey*
[g] *Department of Polymer Science and Technology, Middle East Technical University, 06800 Ankara, Turkey*

ARTICLE INFO

Keywords:
Benzothiadiazole
Fluorene
Organic bulk heterojunction solar cell
Suzuki cross coupling reaction

ABSTRACT

Four novel alternating copolymers bearing 5-fluoro-6-((2-octyldodecyl)oxy)benzo[c][1,2,5]thiadiazole as a strong acceptor unit and 9,9-dioctylfluorene as a strong donor unit with bridging units namely, thienothiophene, selenophene, 3-hexylthiophene, and thiophene were designed and synthesized. The polymers were characterized via ^{1}H NMR spectroscopy, and weight average molecular weights were reported via gel permeation chromatography (GPC). For synthesized novel polymers, the bulk heterojunction solar cells were constructed. Besides, the effects of bridging units on electronic, optical, photovoltaic, and morphological properties were investigated. Among the polymers, the thienothiophene containing polymer P1 exhibited the highest PCE as 4.25% under the illumination of AM 1.5 G with 100 mW/cm^2.

1. Introduction

A couple decades ago, polymers were known as a good insulator until conductive polyacetylene was discovered [1]. With this discovery, both academia and industry show tremendous interest in conducting polymers. Conjugated polymers (CPs) are macromolecules that alter single and double bonds along their skeleton, and they show properties like low-cost, lightweight, solution processability, and flexibility [2]. Therefore, CPs have found many application areas such as biosensors [3], electrochromic devices (EDCs) [4], organic light-emitting diodes (OLED) [5], organic solar cells (OPV) [6], and organic field-effect transistors (OFETs) [7]. In order to control the band gap, which plays a pivotal role in the optoelectronic properties of the conjugated polymers, different approaches are put into practice. The donor–acceptor (D-A) approach is the most effective one among the effects of interchain, planarity, bond-length alternation, and resonance stabilization. For this purpose, different acceptors are introduced into literature like benzo[c][1,2,5]triazole (BTz) [8], benzo[c][1,2,5]thiadiazole (BT) [9], benzo[c][1,2,5]selenadiazole (BS) [10], quinoxaline [11], and isoindigo [12]. BT is one of the most preferred acceptor moieties due to favoring narrow band gaps. It has a strong electron-withdrawing character, which reveals its rigid, planar skeleton containing two imines (-C═N-) bonds. Besides, the dominant quinoid form makes contributions to lower the band gap [13]. Incorporation of substituents like fluorine atoms increases the BT moiety's electron-withdrawing character due to being the most electronegative atom in the periodic table. In addition, the fluorine atom can make noncovalent interactions such as C-F···H and F···S, and its small size reduces the steric hindrance. For the OPV devices, fluorinated BT moiety shows a higher short circuit current and power conversion efficiency, and by lowering the HOMO and LUMO levels exhibits good thermal and oxidative stabilities [14]. The main drawback of the BT moiety is the low solubility. The incorporation of the alkoxy unit containing bulk branched alkyl chains increases the solubility of polymers bearing this unit [15]. Therefore, BT is one of the strongest acceptors to obtain low band gap CP. In the past decade, fluorene derivatives are the most

* Corresponding author at: Chemistry Department, Middle East Technical University, Ankara 06800, Turkey.
E-mail address: toppare@metu.edu.tr (L. Toppare).

https://doi.org/10.1016/j.jelechem.2021.115483
Received 11 May 2021; Received in revised form 18 June 2021; Accepted 18 June 2021
Available online 23 June 2021

commonly used donor moieties for the design of D-A type conjugated polymers. The electron-rich fused aromatic structure of the fluorene reduces the band gap of CP. Besides, fluorene's high electron density makes contributions to absorb larger wavelengths and provides lower oxidation potential [16]. Lately, a new design strategy is introduced, which is the incorporation of π-bridges to the polymer backbone. π-bridges alter the electronic structure and interaction between donor and acceptor units. Hence, such materials directly affect electrochemical, optical, intermolecular charge transport, and photovoltaic characteristics of CP [17]. Therefore, D-π-A type CP can absorb the visible and Near-IR region of the spectrum. Besides, increasing π-π stacking between polymer chains, results in lower band gap. Thiophene and selenophene are the most common π-bridge units in literature. They are electron-rich units that provide absorption of longer wavelengths in the spectrum. However, selenophene has a more stable structure compared to thiophene. Due to selenium's high polarizability, the quinoid character favors more compared to its sulfur counterpart. In addition, the substitution of alkyl chains to the thiophene unit can enhance solubility [18]. 3-hexylthiophene, which has higher solubility, shows similar behavior to thiophene. Thieno[3,2-*b*]thiophene is another π-bridge unit with enhanced π-π stacking that leads to higher hole mobilities. Besides, it provides a linear backbone, which increases the conjugation along the polymer backbone [19]. Therefore, incorporating π-bridge units into the CP backbone shows a significant effect on the organic solar cell device. In this work, a new acceptor core unit 4,7-dibromo-5-fluoro-6-((2-octyldodecyl)oxy)benzo[c][1,2,5]thiadiazole is synthesized and coupled with different π-bridging units; thiophene, selenophene, 3-hexylthiophene, and thieno[3,2-*b*]thiophene. These four units coupled with fluorene donor moiety via Pd catalyzed Suzuki cross-coupling reactions. Herein, electrochemical, spectroelectrochemical, kinetic studies, and OPV device performance of these novel four polymers are explored. Density Functional Theory calculations were used to elucidate experimental results on the theoretical models .

2. Experimental

2.1. General

For the syntheses of all polymers, the chemicals were purchased from Sigma-Aldrich apart from 4,5-Difluoro-2-nitroaniline, purchased from Tokyo Chemical Industry (TCI). 4,5-Difluorobenzene-1,2-diamine, 5,6-difluorobenzo[c][1,2,5]thiadiazole, 4,7-dibromo-5,6-difluorobenzo[c][1,2,5]thiadiazole, 4,7-dibromo-5-fluoro-6-((2-octyldodecyl)oxy)benzo[c][1,2,5]thiadiazole, tributyl(thieno[3,2-*b*]thiophen-2-yl)stannane, 5-fluoro-6-((2-octyldodecyl)oxy)-4,7-bis(thieno[3,2-*b*]thiophen-2-yl)benzo[c][1,2,5]thiadiazole, tributyl(4-hexylthiophen-2-yl)stannane, 5-fluoro-4,7-bis(4-hexylthiophen-2-yl)-6-((2 octyldodecyl)oxy)benzo[c][1,2,5]thiadiazole, tributyl(thiophen-2-yl)stannane, 5-fluoro-6-((2-octyldodecyl)oxy)-4,7-di(thiophen-2-yl)benzo[c][1,2,5]thiadiazole were synthesized according to previously described procedures [20]. Synthetic routes for monomers and polymers were illustrated in Scheme 1 and Scheme 2MB-SPS-800 solvent drying system was utilized to obtain dry solvents. For purification of the synthesized chemicals, column chromatography was performed using Merck Silica Gel 60 with a pore size of 0.040–0.063 mm. The ^{1}H and ^{13}C NMR characterization of the chemicals was conducted by Bruker Spectrospin Avance DPX-400 Spectrometer. In addition, HRMS measurement of the monomers was performed by Waters Synapt G1 High-Definition Mass Spectrometer. Electrochemical characterization was carried out by using GAMRY Reference 600 potentiostat in a three-electrode cell system. These electrodes were the platinum wire used as a counter electrode, the silver wire used as a reference electrode, and Indium Tin Oxide (ITO) coated glass slide used as a working electrode. Electrochemical studies performed in 0.1 M acetonitrile/dichloromethane solvent combination containing tetrabutylammonium hexafluorophosphate as a supporting electrolyte. Cyclic voltammetry was used to determine redox potentials and HOMO-LUMO energy levels. The Jasco V-770 Spectrometer was utilized to determine spectroelectrochemical and kinetic features of the polymers.

2.2. Computational methods

Density functional theory (DFT) calculations were performed for tetramers having the structure of DBABDBABDBABDBAB (D: donor, A: acceptor, B: bridge) with 4 donors, 4 acceptors and 8 bridge structures to represent P1, P2, P3 and P4 models at the B3LYP hybrid functional and 6-311G(d) basis set level adopting tight convergence criteria at 10–8 for RMS density matrix convergence and 10–6 for energy in the Gaussian09 (Revision A.02) software package [21222324]. Comparable agreement with experimental results was obtained with experimental results at this quality of calculations for conducting copolymer studies [25262728]. Alkyl side chains on the alkoxy groups were replaced with ethyl groups to achieve better computational capacity and efficiency balance. Geometry optimizations were started from at least six different initial structures by altering torsional angle between connected donor, bridge and acceptor units to achieve lowest energy geometry. Electrostatic potential surface (ESP), highest occupied molecular orbitals (HOMO), and lowest unoccupied molecular orbitals (LUMO) were calculated and mapped onto the optimized geometries of tetramers. Band gap (E_g) was determined by using two different methods that are direct calculation of energy difference between the HOMO and LUMO for the optimized ground state, and the optical E_g by calculating the first vertical excitation energy of the lowest singlet excited state ($S_0 \rightarrow S_1$). The singlet excited states were calculated by using time-dependent density-functional theory (TDDFT). Vertical ionization potential (VIP) and adiabatic ionization potential (AIP) were calculated by the energy difference between the neutral tetramer and cation state of the optimized ground state geometry, followed by optimized cation geometry, respectively. Vertical Electron Affinity (VEA) and Adiabatic Electron Affinity (AEA) were also calculated by considering the transition from the neutral ground state to the anion at the ground state and optimized anion charged geometry. Hole reorganization energies (λ_{reorg}) were determined based on the formulation by Bredas et al [29]. Total atomic charges (δ) on the two 5-fluoro-6-((2-octyldodecyl)oxy)benzo[c][1,2,5]thiadiazole acceptor, two fluorene donor and four bridging units in the middle part of the tetramer were calculated by using ESP fitting scheme of Merz-Singh-Kollman (MK) [30]. Dipole moment (μ), isotropic polarizability (α) and static hyperpolarizability (β) were calculated for the BABDB type optimized units.

2.3. Synthetic route for tributyl(selenophen-2-yl)stannane

In a three-necked round bottom flask, selenophene (2.10 g, 16.0 mmol) was dissolved in freshly distilled THF under inert atmosphere. Then, the reaction temperature was set to −78 °C, and dropwise addition of *n*-BuLi (7.05 mL, 2.5 M in hexane, 17.6 mmol) was performed, and the mixture was stirred at −78 °C for 2 h. Then, $SnBu_3Cl$ (4.78 mL, 17.6 mmol) was introduced to the reaction mixture by dropwise addition, and the mixture was stirred at room temperature for 12 h. Through the removal of the THF by rotary evaporation, crude was dissolved in DCM and washed with brine and distilled water. The collected organic layers were dried over $MgSO_4$. The desired light-yellow liquid product was obtained with the evaporation of DCM. Yield 95%.^{1}H NMR (400 MHz, $CDCl_3$) δ 8.36 (d, J = 4.3 Hz, 1H), 7.51 (d, J = 3.8 Hz, 1H), 7.49 (d, J = 3.5 Hz, 1H), 1.77 – 1.46 (m, 8H), 1.35 (t, J = 14.7, 8H), 1.19 – 1.02 (m, 8H), 0.91 (q, J = 7.0 Hz, 12H).^{13}C NMR (100 MHz, $CDCl_3$) δ 143.60, 137.90, 135.29, 130.54, 28.98, 27.82, 27.28, 13.66, 11.12.

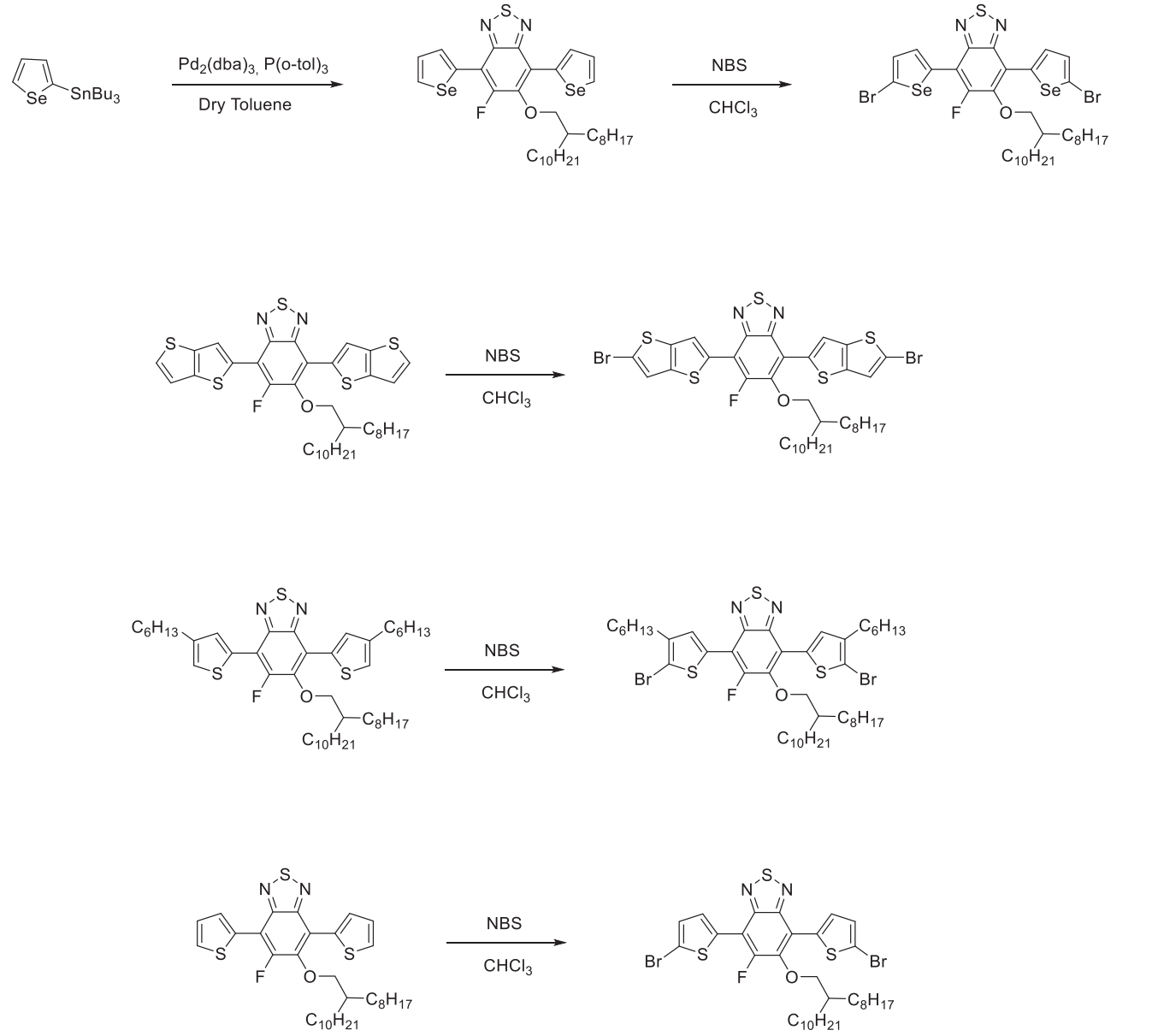

Scheme 1. Synthetic routes for monomers.

2.4. Synthetic route for 5-fluoro-6-((2-octyldodecyl)oxy)-4,7-di (selenophen-2-yl)benzo[c][1,2,5]thiadiazole

In a two-necked round bottom flask, 4,7-dibromo-5-fluoro-6-((2-octyldodecyl)oxy)benzo[c][1,2,5]thiadiazole (0.57 g, 0.94 mmol) and tributyl(selenophen-2-yl)stannane (0.96 g, 2.34 mmol) were mixed in 25 mL dry toluene under an inert atmosphere. After stirring 1 h, bis(dibenzylideneacetone) palladium (0) (44.4 mg, 47.0 μmol) and tri(o-tolyl)phosphine (57.0 mg, 0.19 mmol) were added. The temperature was set to 110 °C, and the mixture was refluxed for 48 h. With the evaporation of the toluene, the desired orange colored product was obtained by column chromatography purification using eluent 1:7 DCM:hexane. Yield 39%. ^{1}H NMR (400 MHz, $CDCl_3$) δ 8.80 (d, J = 3.4 Hz, 1H), 8.49 (d, J = 3.9 Hz, 1H), 8.30 (d, J = 5.7 Hz, 1H), 8.25 (d, J = 5.7 Hz, 1H), 7.48 (dd, J_1 = 5.7, J_2 = 4.1 Hz, 2H), 4.04 (d, J = 6.2 Hz, 2H), 2.10 – 1.99 (m, 1H), 1.65 – 1.50 (m, 4H), 1.29 (s, 28H), 0.90 (s, 6H).^{13}C NMR (100 MHz, $CDCl_3$) δ 154.8, 154.8, 152.2, 148.6, 148.6, 148.3, 148.3, 148.2, 148.2, 145.5, 145.3, 136.4, 135.4, 135.4, 133.3, 133.2, 132.7, 132.0, 131.3, 131.2, 128.7, 128.5, 117.7, 117.7, 112.0, 111.9, 76.8, 38.0, 30.9, 29.8, 29.0, 28.6, 28.6, 28.6, 28.3, 25.6, 21.6, 13.1. HRMS (ESI, m/z), $[M + H]^+$: for $C_{34}H_{46}FN_2OS_3Br_2$ calculated 709.1831 found 709.1848.

2.5. Synthetic route for 4,7-bis(5-bromoselenophen-2-yl)-5-fluoro-6-((2-octyldodecyl)oxy)benzo[c][1,2,5]thiadiazole

5-Fluoro-6-((2-octyldodecyl)oxy)-4,7-di(selenophen-2-yl)benzo[c][1,2,5]thiadiazole (0.30 g, 0.42 mmol) was dissolved in 25 mL chloroform, and N-bromosuccinimide (0.15 g, 0.85 mmol) was added in one portion under dark atmosphere. After stirring at room temperature for 4 h, the chloroform was vaporized under reduced pressure. The residue was extracted with DCM. The combined organic parts were washed with distilled water and dried over $MgSO_4$. After evaporation of the chloroform under reduced pressure, the crude product was purified by column chromatography on silica gel using eluent 1:4 DCM: hexane. Yield 95%.^{1}H NMR (400 MHz, $CDCl_3$) δ 8.55 (d, J = 4.4 Hz, 1H), 8.06 (d, J = 4.4 Hz, 1H), 7.36 (t, J = 4.3 Hz,

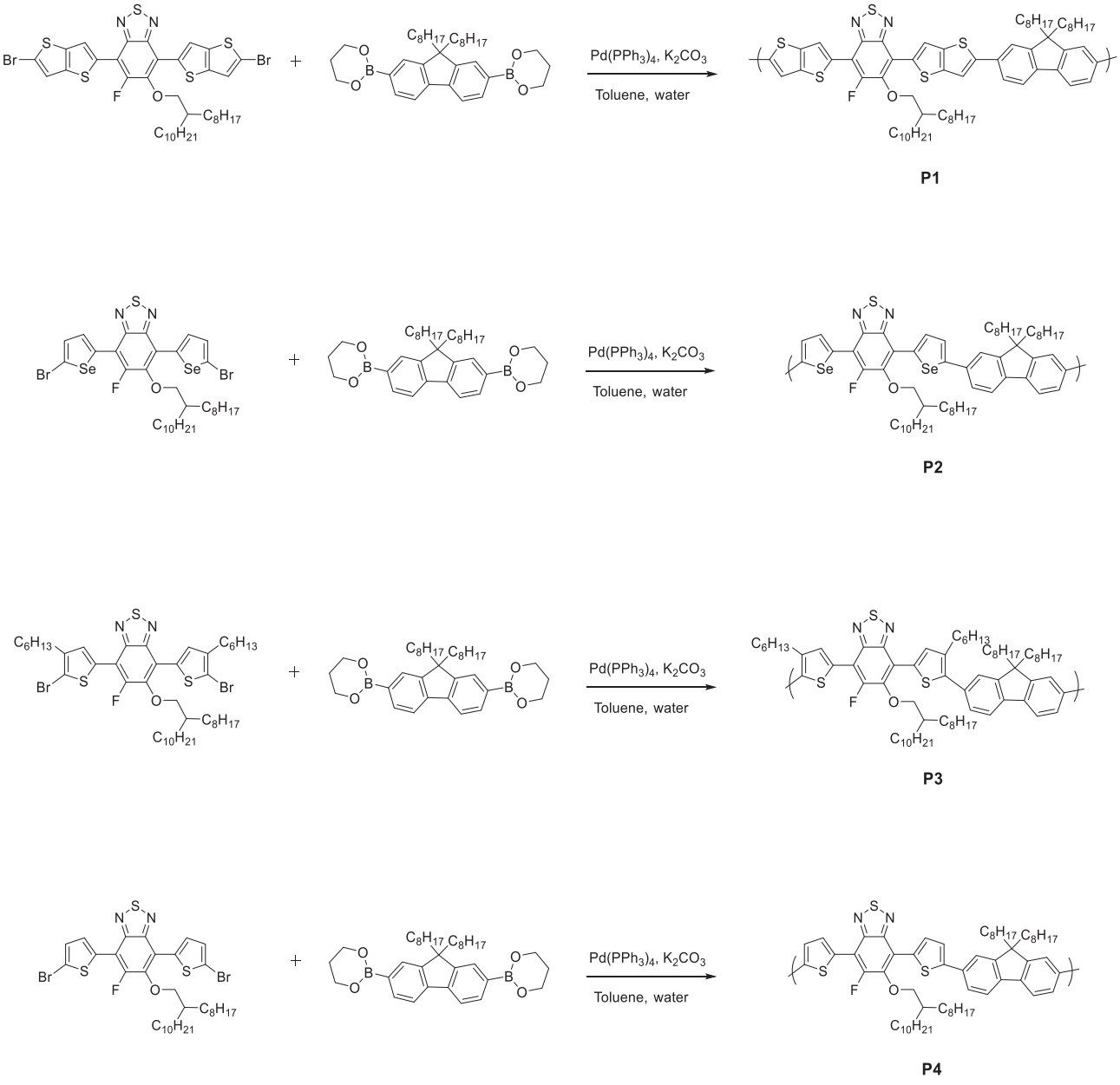

Scheme 2. Synthetic routes for polymers.

2H), 4.02 (d, J = 6.3 Hz, 2H), 2.12 – 2.01 (m, 1H), 1.64 – 1.41 (m, 4H), 1.28 (d, J = 3.1 Hz, 28H), 0.89 (d, J = 4.6 Hz, 6H). ^{13}C NMR (100 MHz, $CDCl_3$) δ 155.6, 153.0, 149.0, 148.8, 146.3, 146.1, 139.1, 139.1, 138.4, 138.3, 133.2, 132.9, 132.9, 132.2, 132.0, 121.4, 121.3, 120.7, 118.0, 112.5, 112.4, 78.2, 78.2, 39.0, 31.8, 30.7, 29.9, 29.6, 29.5, 29.5, 29.2, 26.5 , 22.5, 14.0. HRMS (ESI, *m/z*), $[M + H]^+$: for $C_{34}H_{45}FN_2OS_3Se_2Br_2$ calculated 865.9934 found 866.0013.

2.6. Synthetic route for 4,7-bis(5-bromothieno[3,2-b]thiophen-2-yl)-5-fluoro-6-((2-octyldodecyl)oxy)benzo[c][1,2,5]thiadiazole

5-Fluoro-6-((2-octyldodecyl)oxy)-4,7-bis(thieno[3,2-*b*]thiophen-2-yl)benzo[c][1,2,5]thiadiazole (0.3 g, 0.41 mmol) was dissolved in 25 mL chloroform, and N-bromosuccinimide (0.15 g, 0.83 mmol) was added in one portion under dark atmosphere. After stirring at room temperature for 4 h, the chloroform was vaporized under reduced pressure. The residue was extracted with DCM. The combined organic parts were washed with distilled water and dried over $MgSO_4$. After evaporation of the chloroform, the crude solid was recrystallized in methanol, and the desired product was obtained. Yield 88%. ^{1}H NMR (400 MHz, $CDCl_3$) δ 8.62 (s, 1H), 8.40 (s, 1H), 7.28 (s, 1H), 7.27 (s, 1H), 4.01 (d, J = 6.1 Hz, 2H), 2.06 – 1.99 (m, 1H), 1.61 – 1.48 (m, 4H), 1.28 (s, 28H), 0.89 (d, J = 5.2 Hz, 6H).^{13}C NMR (100 MHz, $CDCl_3$) δ 155.9, 153.3, 149.6, 148.9, 148.7, 146.7, 146.5, 140.4, 140.3, 139.5, 139.3, 134.6, 134.6, 133.3, 133.3, 122.4, 121.9, 121.8, 117.0, 115.3, 115.0, 111.4, 111.3, 78.0, 38.9, 31.8, 30.8, 30.0, 29.6, 29.6, 29.6, 29.5, 29.3, 29.2, 26.6, 22.6, 14.0. HRMS (ESI, *m/z*), $[M + H]^+$: for $C_{38}H_{45}FN_2OS_5Br_2$ calculated 884.0466 found 884.0522.

2.7. Synthetic route for 4,7-bis(5-bromo-4-hexylthiophen-2-yl)-5-fluoro-6-((2-octyldodecyl)oxy)benzo[c][1,2,5]thiadiazole

5-Fluoro-6-((2-octyldodecyl)oxy)-4,7-bis(4-hexylthiophen-2-yl) benzo[c][1,2,5]thiadiazole (0.19 g, 0.24 mmol) was dissolved in

25 mL chloroform, and N-bromosuccinimide (87.35 mg, 0.49 mmol) was added in one portion under dark atmosphere. After stirring at room temperature for 4 h, the chloroform was vaporized under reduced pressure. The residue was extracted with DCM. The combined organic parts were washed with distilled water and dried over $MgSO_4$. After evaporation of the chloroform under reduced pressure, the crude product was purified by column chromatography on silica gel using eluent 1:6 DCM: hexane. Yield 94%. ^{1}H NMR (400 MHz, $CDCl_3$) δ 8.23 (s, 1H), 7.92 (s, 1H), 4.00 (d, J = 5.9 Hz, 2H), 2.64 (t, J = 7.7 Hz, 4H), 2.00 (dd, J_1 = 11.6, J_2 = 5.7 Hz, 1H), 1.69 – 1.63 (m, 4H), 1.37 – 1.25 (m, 44H), 0.89 (m, J = 7.0, 5.5 Hz, 12H). ^{13}C NMR (100 MHz, $CDCl_3$) δ 155.8, 153.3, 149.5, 148.9, 148.8, 146.5, 146.4, 142.1, 141.7, 132.9, 131.7, 131.1, 131.0, 116.3, 113.3, 113.2, 113.1, 110.7, 110.5, 77.9, 38.9, 31.8, 31.5, 31.5, 30.8, 29.9, 29.7, 29.6, 29.5, 29.5, 29.4, 29.2, 28.9, 28.8, 26.6, 22.6, 14.0. HRMS (ESI, m/z), $[M + H]^+$: for $C_{46}H_{70}FN_2OS_3Br_2$ calculated 941.2981 found 941.2979.

2.8. Synthetic route for 4,7-bis(5-bromothiophen-2-yl)-5-fluoro-6-((2-octyldodecyl)oxy)benzo[c][1,2,5]thiadiazole

5-Fluoro-6-((2-octyldodecyl)oxy)-4,7-bis(thieno[3,2-*b*]thiophen-2-yl)benzo[c][1,2,5]thiadiazole (0.3 g, 0.41 mmol) was dissolved in 25 mL chloroform, and N-bromosuccinimide (0.15 g, 0.83 mmol) was added in one portion under dark atmosphere. After stirring at room temperature for 4 h, the chloroform was vaporized under reduced pressure. The residue was extracted with DCM. The combined organic parts were washed with distilled water and dried over $MgSO_4$. After evaporation of the chloroform under reduced pressure, the crude solid was recrystallized in methanol, and the desired product was obtained. Yield 88%. ^{1}H NMR (400 MHz, $CDCl_3$) δ 8.62 (s, 1H), 8.40 (s, 1H), 7.28 (s, 1H), 7.27 (s, 1H), 4.01 (d, J = 6.1 Hz, 2H), 2.06 – 1.99 (m, 1H), 1.61 – 1.48 (m, 4H), 1.28 (s, 28H), 0.89 (d, J = 5.2 Hz, 6H). ^{13}C NMR (101 MHz, $CDCl_3$) δ 155.9, 153.3, 149.6, 148.9, 148.7, 146.7, 146.5, 140.4, 140.3, 139.5, 139.3, 134.6, 134.6, 133.3, 133. 3, 122.4, 121.9, 121.8, 117.0, 115.3, 115.0, 111.4, 111.3, 78.0, 38.9, 31.8, 30.8, 30.0, 29.6, 29.6, 29.6, 29.5, 29.3, 29.2, 26.6, 22.6, 14.0. HRMS (ESI, m/z), $[M + H]^+$: for $C_{38}H_{45}FN_2OS_5Br_2$ calculated 884.0466 found 884.0522.

2.9. Synthetic route for P1

4,7-bis(5-bromothieno[3,2-*b*]thiophen-2-yl)-5-fluoro-6-((2-octyldodecyl)oxy)benzo[c][1,2,5]thiadiazole (0.10 g, 0.11 mmol), 9,9-Dioctylfluorene-2,7-diboronic acid bis(1,3-propanediol) ester (63.1 mg, 0.11 mmol), 0.14 mL 2 M K_2CO_3, 1–2 drops Aliquat 336, and $Pd(PPh_3)_4$ (5 mol%) were poured in a 50 mL schlenk tube, and stirred under argon atmosphere for 2 h. Then, 15 mL dry toluene was added and heated to reflux for 72 h. After removal of the toluene, the crude was extracted with chloroform and washed with distilled water. The combined organic parts were dried over $MgSO_4$, and the solvent was evaporated under reduced pressure. Then, cold methanol and sodium diethyldithiocarbamate (Pd scavenger) was added to the crude and stirred for 1.5 h. The polymer was then filtered through a soxhlet extractor and washed with methanol, acetone, and hexane to eliminate the low molecular weight oligomers. Chloroform was used to gather polymer as a dark purple colored solid. Yield 47%. ^{1}H NMR (400 MHz, $CDCl_3$) δ 8.57, 8.25, 7.58, 7.52, 7.37, 7.32, 6.98, 6.81, 4.12, 4.10, 1.42–1.26, 0.94–0.81. Mw: 79 kDa, Mn: 55 kDa, PDI: 1.43.

2.10. Synthetic route for P2

4,7-bis(5-bromoselenophen-2-yl)-5-fluoro-6-((2-octyldodecyl)oxy) benzo[c][1,2,5]thiadiazole (0.10 g, 0.12 mmol), 9,9-Dioctylfluorene-2,7-diboronic acid bis(1,3-propanediol) ester (64.4 mg, 0.12 mmol), 0.13 mL 2 M K_2CO_3, 1–2 drops Aliquat 336, and $Pd(PPh_3)_4$ (5 mol %) were poured in a 50 mL schlenk tube, and stirred under argon atmosphere for 2 h. Then, 15 mL dry toluene was added and heated to reflux for 72 h. After removal of the toluene, the crude was extracted with chloroform and washed with distilled water. The combined organic parts were dried over $MgSO_4$, and the solvent was evaporated under reduced pressure. Then, cold methanol and sodium diethyldithiocarbamate (Pd scavenger) were added to the medium and stirred for 1.5 h. The polymer was then filtered through a soxhlet extractor and washed with methanol, acetone to eliminate the low molecular weight oligomers. Hexane was used to gather polymer as a dark purple colored solid. Yield 54%. ^{1}H NMR (400 MHz, $CDCl_3$) δ 8.84, 8.50, 7.71–7.65, 4.14, 2.34, 2.10, 1.66, 1.55, 1.28, 1.12, 0.89, 0.81–0.80. Mw: 27 kDa, Mn: 16 kDa, PDI: 1.66.

2.11. Synthetic route for P3

4,7-bis(5-bromo-4-hexylthiophen-2-yl)-5-fluoro-6-((2-octyldodecyl)oxy)benzo[c][1,2,5]thiadiazole (0.10 g, 0.11 mmol), 9,9-Dioctylfluorene-2,7-diboronic acid bis(1,3-propanediol) ester (59.3 mg, 0.11 mmol), 0.13 mL 2 M K_2CO_3, 1–2 drops Aliquat 336, and $Pd(PPh_3)_4$ (5 mol%) were poured in a 50 mL schlenk tube, and stirred under argon atmosphere for 2 h. Then, 15 mL dry toluene was added and heated to reflux for 72 h. After removal of the toluene, the crude was extracted with chloroform and washed with distilled water. The combined organic parts were dried over $MgSO_4$, and the solvent was evaporated under reduced pressure. Then, cold methanol and sodium diethyldithiocarbamate (Pd scavenger) were added to the medium and stirred for 1.5 h. The polymer was then filtered through a soxhlet extractor and washed with methanol, acetone to eliminate the low molecular weight parts. Hexane was used to gather polymer as a dark orange colored solid. Yield 16%. ^{1}H NMR (400 MHz, $CDCl_3$) δ 8.43–8.41, 8.29, 8.20–8.17, 8.13, 7.99, 7.83–7.80, 7.56–7.54, 7.38–7.35, 7.19, 7.14, 6.87, 4.12–4.08, 2.84, 2.76–2.68, 2.07, 1.76, 1.60, 1.31–1.27, 1.13, 0.87–0.81. Mw: 4 kDa, Mn: 3 kDa, PDI: 1.43.

2.12. Synthetic route for P4

4,7-bis(5-bromothieno[3,2-*b*]thiophen-2-yl)-5-fluoro-6-((2-octyldodecyl)oxy)benzo[c][1,2,5] thiadiazole (0.10 g, 0.11 mmol), 9,9-Dioctylfluorene-2,7-diboronic acid bis(1,3-propanediol) ester (63.1 mg, 0.11 mmol), 0.14 mL 2 M K_2CO_3, 1–2 drops Aliquat 336, and $Pd(PPh_3)_4$ (5 mol%) were poured in a 50 mL schlenk tube, and stirred under argon atmosphere for 2 h. Then, 15 mL dry toluene was added and heated to reflux for 72 h. After removal of the toluene, the crude was extracted with chloroform and washed with distilled water. The combined organic parts were dried over $MgSO_4$, and the solvent was evaporated under reduced pressure. Then, cold methanol and sodium diethyldithiocarbamate (Pd scavenger) were added to the medium and stirred for 1.5 h. The polymer was then filtered through a soxhlet extractor and washed with methanol, acetone to eliminate the low molecular weight oligomers. Hexane was used to gather polymer as a dark purple colored solid. Yield 47%. ^{1}H NMR (400 MHz, $CDCl_3$) δ 8.52, 8.32, 7.76–7.72, 7.55, 4.13, 2.09, 1.66–1.62 1.53, 1.27, 1.11, 0.87, 0.80–0.79. Mw: 13 kDa, Mn: 7kDa Da, PDI: 1.75.

3. Result and discussion

3.1. Electrochemical studies

Cyclic Voltammetry is a crucial tool for exploring oxidation–reduction behavior and HOMO/LUMO energy levels of the conjugated copolymers. These electrochemical behaviors are determined using a three-electrode cell system, and the electrodes are namely platinum

wire as a counter, silver wire as a reference, and ITO coated glass slide as a working electrode.

In order to carry out cyclic voltammetry studies, polymers P1, P2, P3, and P4 were dissolved in chloroform to adjust a concentration of 5 mg/mL, and then spray coated onto the working electrode surface via a spray gun. Electrochemical studies were performed in a 0.1 M $TBAPF_6$ /ACN supporting electrolyte/solvent combination at a 100 $mV.s^{-1}$ scan rate. The single scan cyclic voltammetry of the polymers was run in the potential range between 0.00 V /1.60 V for P1, 0.00 V /1.65 V for P2, −1.60 V /1.70 V for P3, and −2.10 V /1.60 V for P4, respectively (Fig. 1). The polymers' redox potentials at doping /doped state were determined as 1.20 V /0.95 V for P1, and 1.50 V /1.12 V for P2, 1.60 V /1.25 V for P3, and 1.45 V /1.00 V for P4 (Table 1). The polymers P3 and P4 showed ambipolar character (both p-dope and *n*-dope behavior). Even P4 shows reversible two *n*-doped states. *N*-doping/*n*-dedoping potentials were −1.36 V /-1.21 V for P3, and −1.29 V /-1.21 V, and −1.91 V /-1.68 V for P4, respectively.

In this work, different π bridging units thieno[3,2-*b*]thiophene, selenophene, 3-hexylthiophene, and thiophene) were incorporated into the polymer backbone in order to compare the electrochemical behavior of the polymers. The different oxidation potentials of the polymers can be explained by electronic nature and different electron densities of the π bridging units. The thieno[3,2-*b*]thiophene comprising polymer (P1) exhibited the lowest oxidation potential as 1.20 V among the other polymers. This is because of thieno[3,2-b]thiophene's high electron density nature and high electron-donating ability compared to other bridging units. The highest oxidation potential belongs to P3 as 1.60 V. In literature, it is stated that the 3-hexylthiophene comprising polymers exhibit higher oxidation potential values compared to others [31]. Besides, the bulky alkyl chain of 3-hexylthiophene sterically hinders the coplanarity between adjacent rings, which results in high oxidation potential.

HOMO/LUMO energy levels characterization plays a crucial role in investigating the conjugated polymer application fields. HOMO energy levels of the polymers, P1, P2, P3, and P4, were calculated from the onset of oxidation potentials using equation HOMO = -(4.75 + Eoxonset) and recorded as −5.70 eV, −5.87 eV, −5.90 eV, and −5.89 eV, respectively. LUMO energy levels of the polymers were calculated from the onset of reduction potentials using equation LUMO = -(4.75 + Eredonset) and recorded as −3.80 eV, −4.00 eV, −3.80 eV, and −3.71 eV, respectively. Electronic band gap (E_g^{el}) was calculated using the equation E_g^{el} = HOMO-LUMO and the lowest HOMO energy level belongs to the P1 among the other polymers. Since thieno[3,2-*b*]thiophene has higher electron density with an extended conjugation and higher electron-donating ability compared to selenophene, thiophene, and 3-hexylthiophene. P2, which comprises the selenophene unit, has the second-lowest HOMO energy level. It can be explained by selenium's high polarizability compared to its sulfur counterpart, which favors quinoid structure more and lowers HOMO energy level. Therefore, selenophene comprising polymer, namely P2, has a lower HOMO energy level than thiophene comprising polymer, namely P4. 3-Hexylthiophene comprising polymer, namely P3, has the highest HOMO energy level due to above-mentioned reason.

The scan rate dependences of the polymers were investigated at a single scan cyclic voltammogram were reported at four scan rates (50 $mV.s^{-1}$, 100 $mV.s^{-1}$, 150 $mV.s^{-1}$, 200 $mV.s^{-1}$) in 0.1 M $TBAPF_6$ /ACN electrolyte solvent couple (Fig. 2).

The linear relationship of current density to the scan rate was investigated for P1, P2, and P4 (Fig. 3). The linear plot proves the non-diffusion-controlled mass transfer while doping-dedoping process and well-coated polymer film.

3.2. Spectroelectrochemical studies

Spectroelectrochemical works were conducted in order to discover optical properties and electronic changes in the application of stepwise oxidation. The characteristic parameters such as λ_{max}, optical band gap (E_g^{op}), polaron and bipolaron regions were determined from UV–Vis-NIR absorption spectra of the polymers. Absorption spectra of the

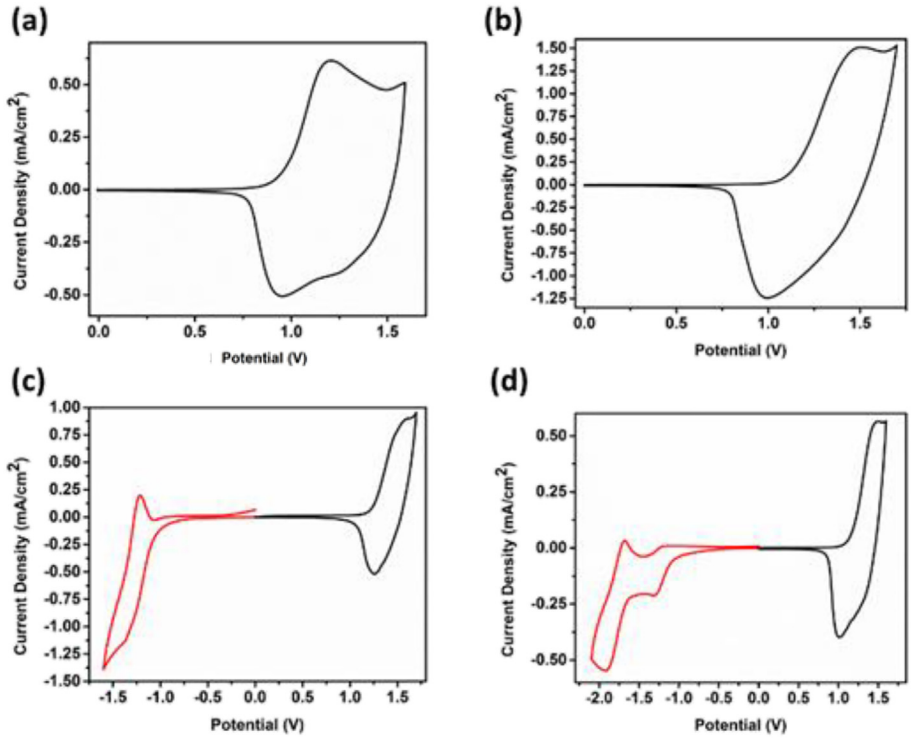

Fig. 1. Single scan cyclic voltammetry of the polymers (a) P1, (b) P2, (c) P3, and (d) P4 in a 0.1 $TBAPF_6$ /ACN electrolyte solution.

Table 1
Electrochemical and Spectroelectrochemical properties of the polymers.

	$E_{p\text{-doping}}$ (V)	$E_{p\text{-dedoping}}$ (V)	$E_{n\text{-}doping}$ (V)	$E_{n\text{-dedoping}}$ (V)	HOMO (eV)	LUMO (eV)	E_g^{op} (eV)	Λ_{max}^{onset} (nm)	Λ_{max} (nm)	Polaron (nm)	Bipolaron (nm)
P1	1.20	0.95	–	–	−5.70	−3.85	1.85	670	403/545	770	1530
P2	1.50	1.12	–	–	−5.87	−4.06	1.81	685	395/543	845	1635
P3	1.60	1.25	−1.36	−1.21	−5.90	−3.80	1.95	636	360/500	740	1570
P4	1.45	1.00	−1.29/−1.91	−1.22/−1.68	−5.89	−3.71	1.73	717	390/555	785	1630

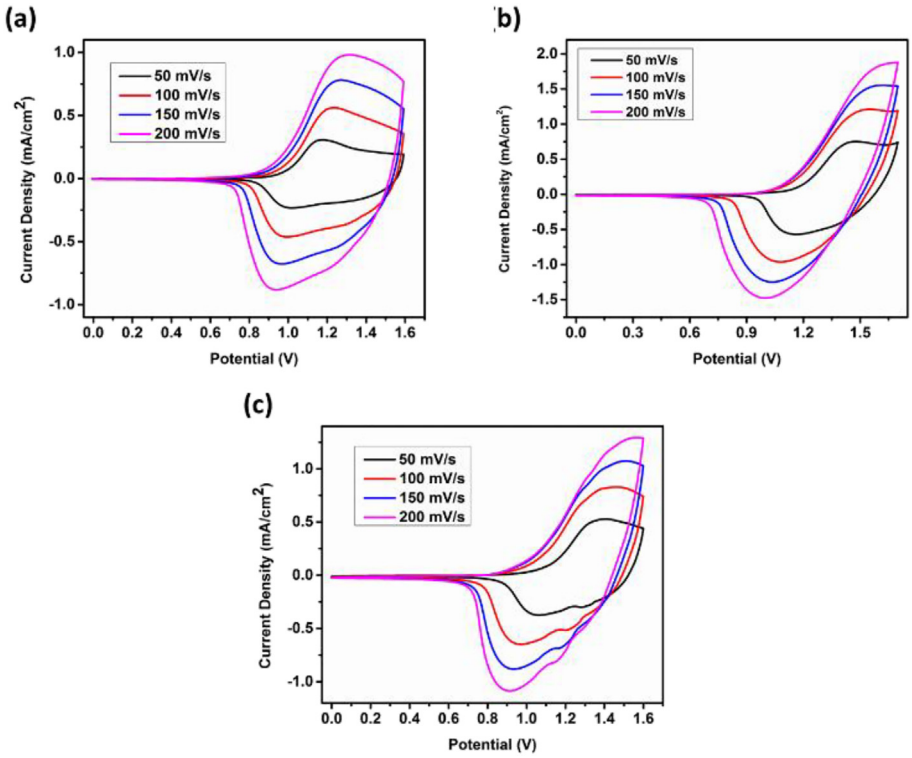

Fig. 2. Scan rate dependences of the polymers (a) P1, (b) P2, and (c) P4 in a 0.1 $TBAPF_6$ /ACN electrolyte solution.

spray-coated polymers onto ITO slides were carried out in a monomer free, 0.1 M $TBAPF_6$ /ACN electrolyte solution using UV–Vis-NIR spectrophotometer coupled with a potentiostat. Spectroelectrochemical characterizations were started by applying −0.5 V constant potential to obtain neutral polymer film, then stepwise oxidation performed between 0.00 V and 1.40 V for P1, 0.00 V and 1.50 V for P2, 0.00 V and 1.60 V for P3, 0.00 V and 1.45 V for P4 (Fig. 4).

The maximum neutral state absorption of the polymers in the visible region of the spectrum were determined at 545 nm for P1, 543 nm for P2, 500 nm for P3, 555 nm for P4. These λ_{max} values were attributed to π- π* transitions. The continuous stepwise oxidation leads to new absorptions which belong to polaron (radical cation) and bipolaron (dication) formation in the NIR region. These new absorption bands are determined at 770 nm, 1530 nm for P1, 845 nm, 1635 nm for P2, 740 nm, 1570 nm for P3, 785 nm, 1630 nm for P4, respectively.

Apart from the λ_{max}, polaron, and bipolaron characteristics, E_g^{op} is another important characteristic parameter to determine the application area of the conjugated polymers. The optical band gap is calculated from the onset of π- π* transitions of the polymer film's neutral state using the equation $E_g^{op} = 1241/\lambda$. The calculated E_g^{op} values are 1.85 eV for P1, 1.81 eV for P2, 1.95 eV for P3, and 1.73 eV for P4 respectively (Table 1). Among four polymers, thiophene comprising polymer showed the red-shifted state absorption at 555 nm with the lowest E_g^{op} value as 1.73 eV. This result can be devoted to thiophenes' low-lying HOMO energy level compared to its selenium counterpart. Selenophene and thieno[3,2-*b*]thiophene comprising polymers showed similar E_g^{op} values as 1.81 eV and 1.85 eV at similar neutral absorption states as 543 nm and 545 nm. These similar results can be dedicated to the high electron-donating ability of both selenophene and thieno[3,2-*b*]thiophene. 3-hexylthiophene comprising polymer has the highest E_g^{op} value as 1.95 eV, which can be devoted to the polymer's low molecular weight. This is probably due to containing a sterically bulky alkyl chain in 3-hexylthiophene which interrupts growth of the chain during polymerization. As the number of repeating units decreases, conjugation length decreases, and hence a higher band gap of the P3 was calculated.

All the polymers exhibited electrochromic character since they have different colors at both neutral and doped states. The electrochromic character is an important feature for conjugated polymers due to large application areas such as displays, smart windows, and glasses. The colors at neutral and doped states were reported in the application of a different constant potential (Fig. 5). The color of the polymers at neutral states were in coherence with the color of neutral state absorptions. The thiophene comprising polymer showed the most red-shifted absorption (555 nm) with a purple color in the neutral state. The 3-hexylthiophene comprising polymer showed most blue-shifted absorption (500 nm) with orange color in the neutral state. Moreover, P1 and P2 exhibited different purple color shades in their

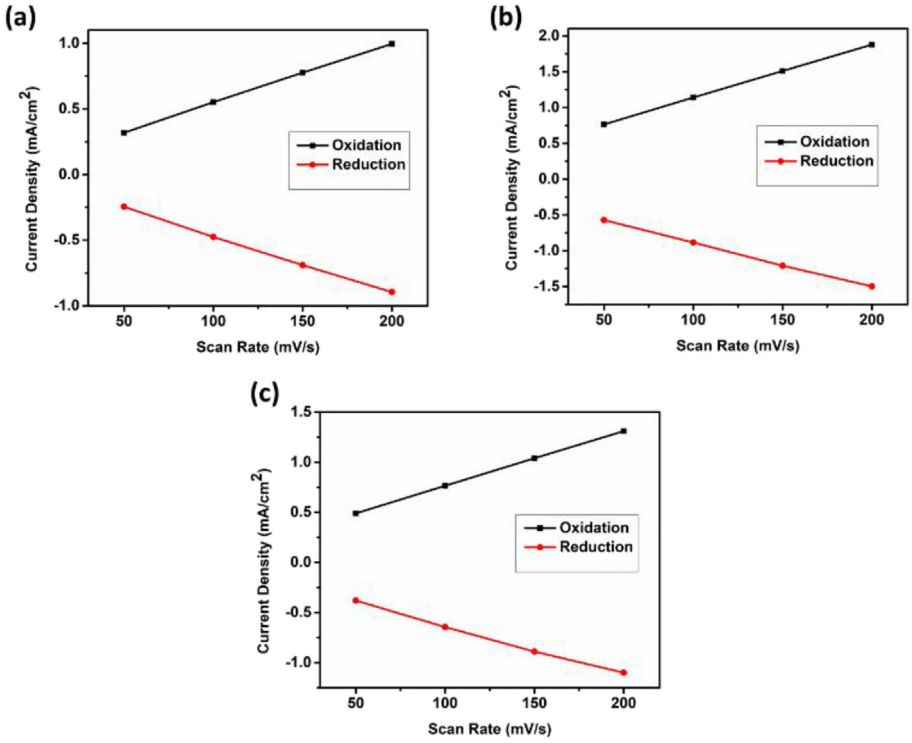

Fig. 3. Current density – scan rate relationship of the polymers (a) P1, (b) P2 and (c) P4 in a 0.1 $TBAPF_6$ /ACN electrolyte solution.

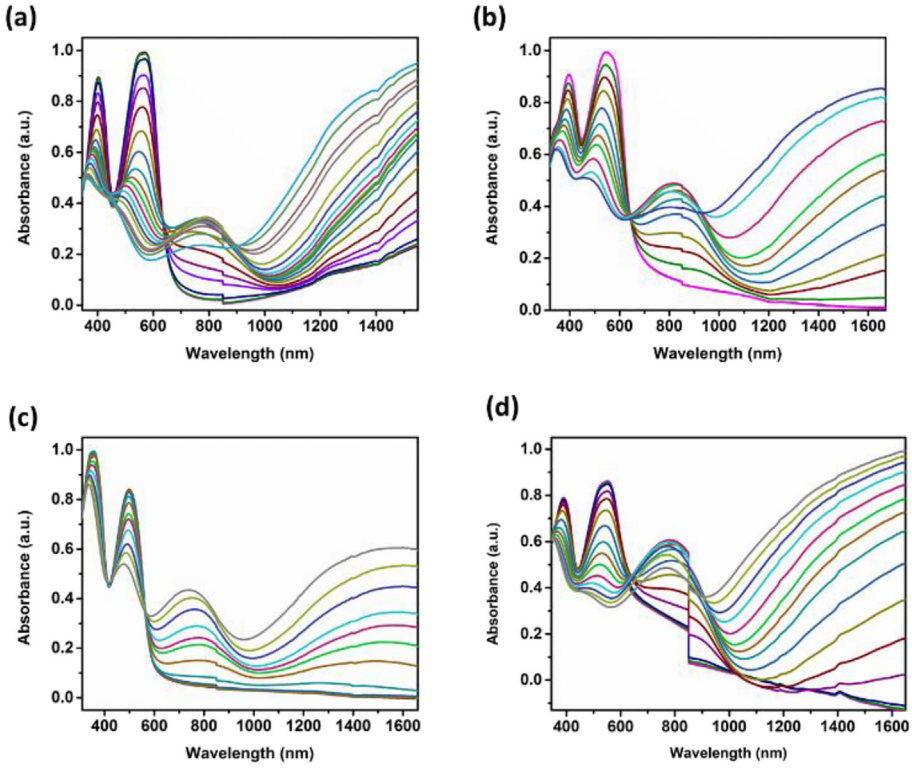

Fig. 4. Electronic absorption spectra of the polymers (a) P1, (b) P2, (c) P3, and (d) P4 in a 0.1 M $TBAPF_6$ /ACN electrolyte solution.

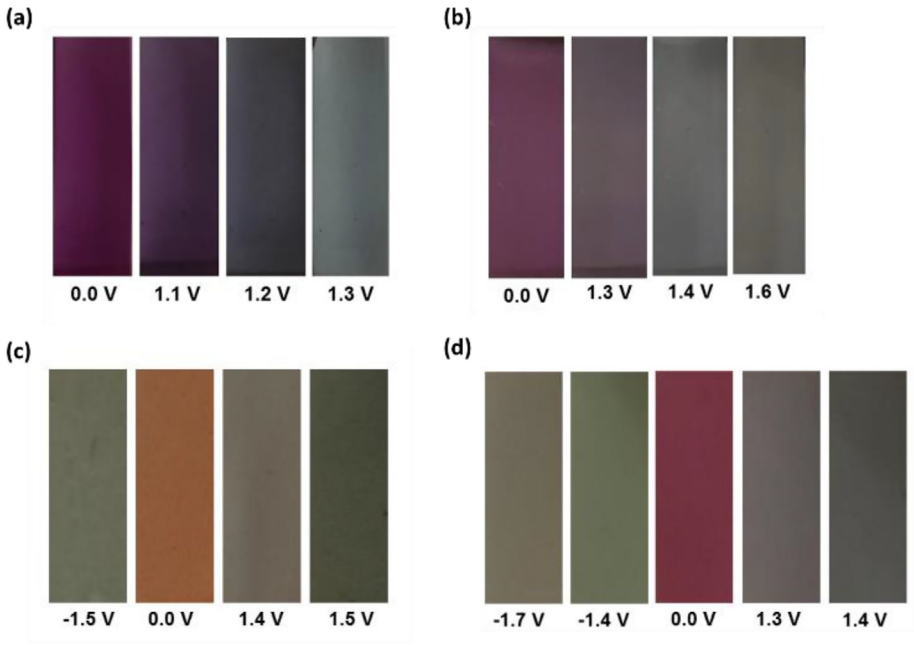

Fig. 5. Different colors of the polymers (a) P1, (b) P2, (c) P3, and (d) P4 at neutral, oxidized, and reduced states.

neutral states at 545 nm and 543 nm, respectively. All polymers showed different grey color shades in their oxidized states, whereas P3 and P4 showed different green color shades in their reduced states.

3.3. Kinetic studies

In order to calculate the switching time and optical contrast of the polymers, kinetic works were conducted. Optical contrast can be defined as the change in the percent transmittance at a certain wavelength, and switching time is time needed to change color between neutral and oxidized states. Kinetic works were carried out at absorption maxima values determined in spectroelectrochemical works in the application of potential within 5 s intervals (Fig. 6). For all polymers optical contrast and switching times were reported at maximum absorption state of neutral, polaron and bipolaron regions (Table 2). The reported values are 34% (at 403 nm) with 1.8 s, 50% (at

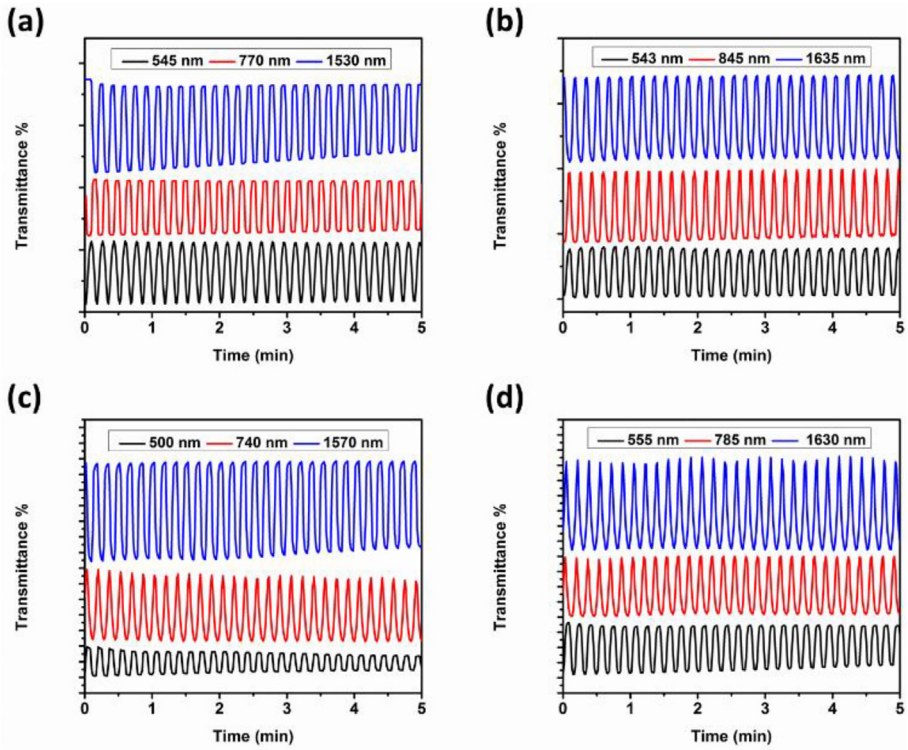

Fig. 6. Change in the percent transmittance observed at the absorption maxima of the polymers (a) P1, (b) P2, (c) P3, and (d) P4 in a 0.1 M $TBAPF_6$ /ACN electrolyte solution.

Table 2
Kinetic properties of the polymers.

	Λ_{max} (nm)	Optical Contrast (%)	Switching Time (s)
P1	545	50	3.4
	770	45	1.7
	1530	71	1.7
P2	543	39	3.1
	845	54	2.7
	1635	65	2.4
P3	500	19	1.5
	740	45	3.8
	1570	63	1.8
P4	555	34	2.8
	785	39	3.4
	1630	61	3.8

Table 3
Optical properties of P1, P2, P3, and P4 in chloroform solution and thin film form.

	Solution Λ (nm)	Thin Film Λ (nm)
P1	403	405
	547	549
P2	393	402
	551	583
P3	340	358
	481	497
P4	379	389
	512	552

545 nm) with 3.4 s, 45% (at 770 nm) with 1.7 s, and 71% (at 1530 nm) with 1.7 s for P1, 29% (at 395 nm) with 2.9 s, 39% (at 543 nm) with 3.1 s, 54% (at 845 nm) with 2.7 s, and 65% (at 1635 nm) with 2.4 s for P2, 19% (at 360 nm) with 1.6 s, 19% (at 500 nm) with 1.5 s, 45% (at 740 nm) with 3.8 s, and 63% (at 1570 nm) with 1.8 s for P3, 20% (at 403 nm) with 3.0 s, 34% (at 545 nm) with 2.8 s, 39% (at 770 nm) with 3.4 s, and 61% (at 1530 nm) with 3.8 s for P4. Among these four polymers, P1 obtained relatively better optical contrast and switching time values compared to other polymers. As is mentioned above, these results can be dedicated to electron-rich nature and better electron-donating ability of thieno[3,2-*b*]thiophene.Table 3.

The absorption spectrum of the polymer solution in chloroform and polymer thin film was obtained using a UV–Vis spectrophotometer (Fig. 7). All polymers exhibited red-shift absorption in thin-film polymers compared to the polymer solution. This red-shift could be explained by reducing conformation change freely, high π-electron delocalization on a planar solid state, or the polymer and solvent interaction.

3.4. Photovoltaic studies

Electrochemical works showed that all polymers have suitable band gaps and HOMO-LUMO energy levels to construct organic bulk heterojunction solar cells. ITO/PEDOT:PSS/Polymer: $PC_{71}BM$/LiF/Al based device architecture was fabricated for all polymers apart from P3. The low yield of the polymerization reaction resulted in the low amount of P3 which was not enough for device fabrication. Current density–voltage (J-V) properties of the BHJ devices were determined under light illumination (AM 1.5 G with 100 mW/cm^2). In order to determine the most efficient devices, a wide variety of optimizations were conducted such as polymer and $PC_{71}BM$ blend ratio (w:w), blend concentration, and thickness optimizations. In order to enhance the device performance, the solvent additive is used and only P1 showed better performance with the addition of DPE as a solvent additive (4.25%). For P2, 2% CN and 3% DPE, and for P4, 2% DIO and 3% DPE additive treatments were performed. However, low PCEs were found and this can be related to morphology. The efficiency of exciton dissociation and transport of charge carriers are directly related to donor and acceptor arrangements on the morphology [3233]. Therefore, the decrease in the PCEs of P2 and P4 could be probably due

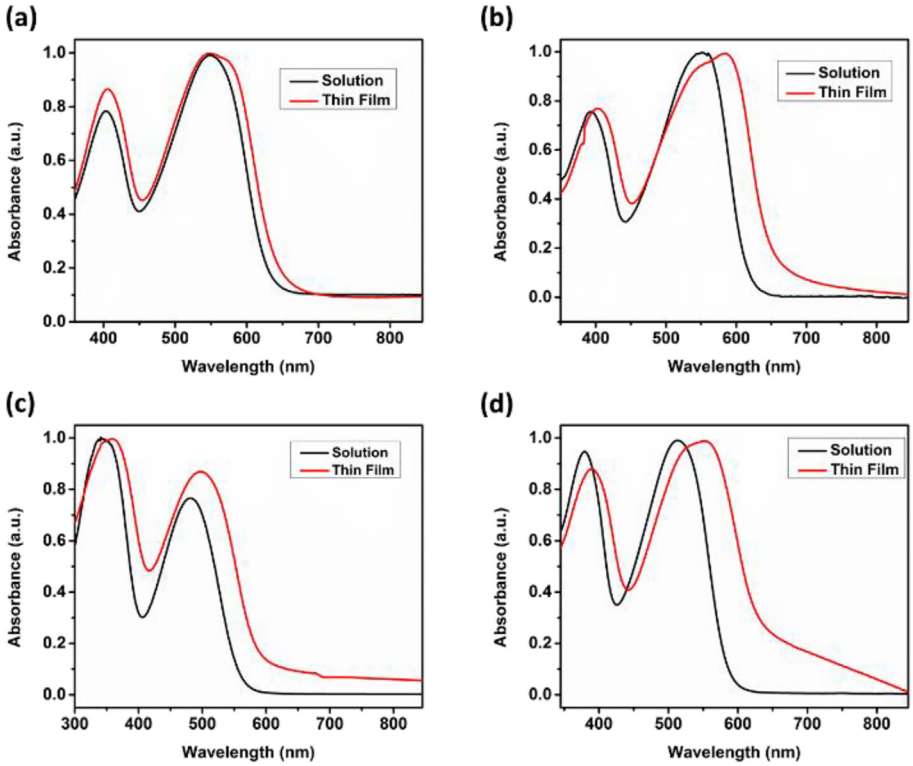

Fig. 7. Absorption spectra of the polymers (a) P1, (b) P2, (c) P3, and (d) P4 solutions in chloroform and polymer thin film.

Table 4
Photovoltaic parameters of P1 based BHJ solar cells.

Polymer(P1):$PC_{71}BM$	J_{SC}	V_{OC}	FF%	PCE%	RPM	Treatment
1:1 (2%)	4.92	0.81	32.78	1.30	750	–
1:2 (2%)	5.14	0.77	41.64	1.66	750	–
1:3 (2%)	5.52	0.78	49.13	2.11	750	–
1:4 (2%)	4.92	0.79	48.37	1.86	750	–
1:3 (2.5%)	5.74	0.79	52.47	2.38	750	–
1:3 (3%)	9.96	0.79	45.61	3.60	750	–
1:3 (3.5%)	9.46	0.80	41.40	3.12	750	–
1:3 (3%)	9.59	0.81	38.81	3.02	500	–
1:3 (3%)	8.19	0.83	46.09	3.14	1000	–
1:3 (3%)	9.03	0.87	44.67	3.53	750	DPE (3%)
1:3 (3%)	10.89	0.82	47.74	4.25	750	DPE (6%)

Table 5
Photovoltaic parameters of P2 based BHJ solar cells.

Polymer(P2):$PC_{71}BM$	J_{SC}	V_{OC}	FF%	PCE%	RPM
1:1 (2%)	2.65	0.80	32.01	0.67	750
1:2 (2%)	4.28	0.79	41.28	1.40	750
1:3 (2%)	3.78	0.79	38.85	1.16	750
1:4 (2%)	3.80	0.74	36.95	1.04	750
1:2 (3%)	6.88	0.81	36.98	2.07	750
1:2 (3.5%)	7.82	0.79	34.25	2.13	750
1:2 (4%)	7.37	0.79	32.00	1.86	750
1:2 (3.5%)	6.54	0.73	33.14	1.58	500
1:2 (3.5%)	8.31	0.74	36.94	2.26	1000

Table 6
Photovoltaic parameters of P4 based BHJ solar cells.

Polymer(P4):$PC_{71}BM$	J_{SC}	V_{OC}	FF%	PCE%	RPM
1:1 (2%)	2.85	0.73	30.74	0.64	750
1:2 (2%)	3.26	0.72	30.45	0.72	750
1:3 (2%)	3.82	0.69	31.86	0.84	750
1:4 (2%)	3.61	0.58	29.92	0.63	750
1:3 (3%)	2.09	0.62	27.77	0.36	750
1:3 (2%)	2.90	0.60	27.90	0.49	500
1:3 (2%)	2.85	0.62	33.52	0.59	1000

to deterioration of the morphology in the presence of additives, whereas the PCE of P1 based solar cells were improved with additive treatment which enhances morphology [34]. All photovoltaic works of the novel three polymers are reported (Table 4, 5, 6).

According to photovoltaic results, the highest performance belongs to thienothiophene containing polymer P1 based solar cells with 1:3 (w:w) P1:$PC_{71}BM$ blend ratio with 3% concentration in addition to 6% DPE with the spin coating rate of 750 rpm. (Fig. 8). This device exhibited the highest PCE as 4.25%, J_{SC} as 10.89 mA/cm^2, V_{OC} as 0.82 V and FF as 47.74%. For selenophene containing polymer P2, the highest PCE was 2.26%, J_{SC} as 8.31 mA/cm^2, V_{OC} as 0.74 V and FF as 36.94%. For thiophene containing polymer P4, the highest PCE was 0.84%, J_{SC} as 3.82 mA/cm^2, V_{OC} as 0.69 V and FF as 31.86%. When the V_{oc} of the copolymers were compared the highest V_{OC} belongs to P1 even though P4 has the deepest HOMO energy level. However, there are other parameters which also have significant impact on the V_{oc}. These parameters are morphology, charge transfer states, recombination, donor/ acceptor interface area, carrier density [35]. In addition to this, donor/acceptor ratio and the thickness of the active layer affects the charge transfer states which is directly related to the V_{OC} [36]. Therefore, higher V_{OC} of P1 can be due to more uniformly distributed morphology of the active layer which is evidenced in TEM images.

The current density- voltage (J-V) curves of the P1 based BHJ devices were reported for blend ratios, concentrations, thickness at different spin coating rates, and additive percent's (Fig. 8). The PCE of P1 is enhanced from 2.11% to 3.60% when the concentration is increased from 2% to 3% at 1:3 blend ratio in the o-DCB solvent at spin coating rate of 750 rpm. As the polymer:$PC_{71}BM$ concentration in the active layer rises, light absorption raises, which leads to better solar performances. With the addition of diphenyl ether (DPE), photovoltaic performance of P1 based solar cells were improved. Since the additive treatment makes enhancement on morphology which leads to easier exciton dissociation and charge transport; thus, photovoltaic efficiency increases [37]. When the DPE concentration is raised from 3% to 6%, the PCE rises to 4.24%. This can be attributed to further improvement of the morphology with 6% additive compared to 3% additive.

For P2 based devices, J-V curves for blend ratio, concentration, and thickness optimizations were demonstrated in Fig. 9. According to photovoltaic data, the J_{SC}, FF and PCE values reduce as the blend ratio alters from 1:2 to 1:4 (Table 5). The device efficiency is improved when concentration is 3.5% in the o-DCB solvent. The best device is obtained with a spin coating rate of 1000 rpm. When the coating rate increases, the J_{sc} value also increases since a thinner active layer makes it easier to transport holes and electrodes to corresponding electrodes [3839]. Finally, the J-V graphs were drawn for P4 based polymers for the study of blend ratio, concentration, and thickness (Fig. 10). The highest PCE value is obtained as 0.84% with the blend ratio of 1:3, 2% concentration in o-DCB solvent at a spin coating rate of 750 rpm (Table 6). When concentration rose from 2% to 3%, PCE reduced from 0.84% to 0.36%. This result can be devoted to reduction of J_{SC} value from 3.82 to 2.09mA/cm^2.

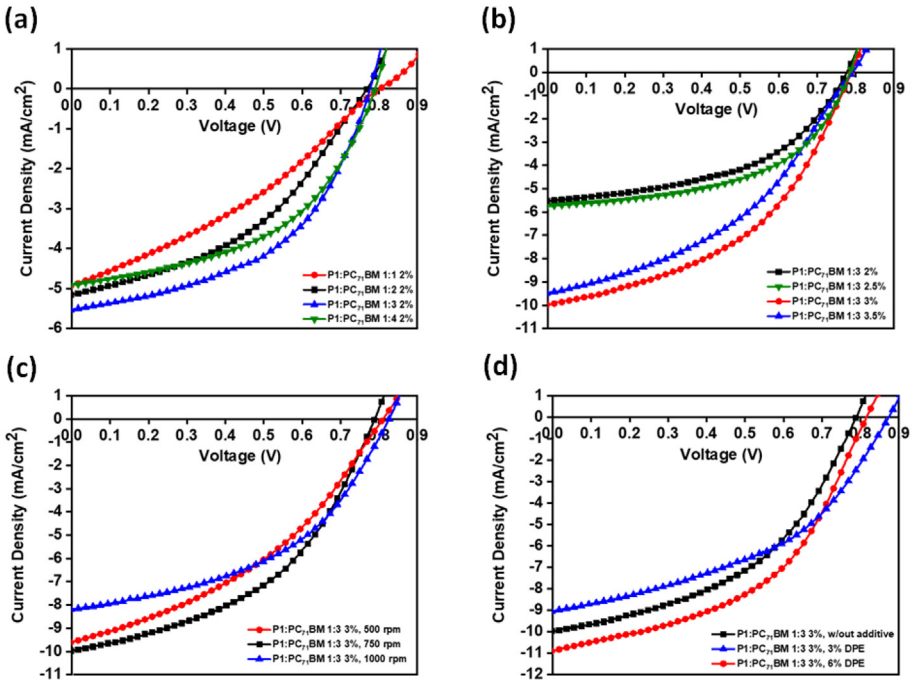

Fig. 8. Current density–voltage curve of P1 for study of a) blend ratio b) concentration c) thickness d) additive.

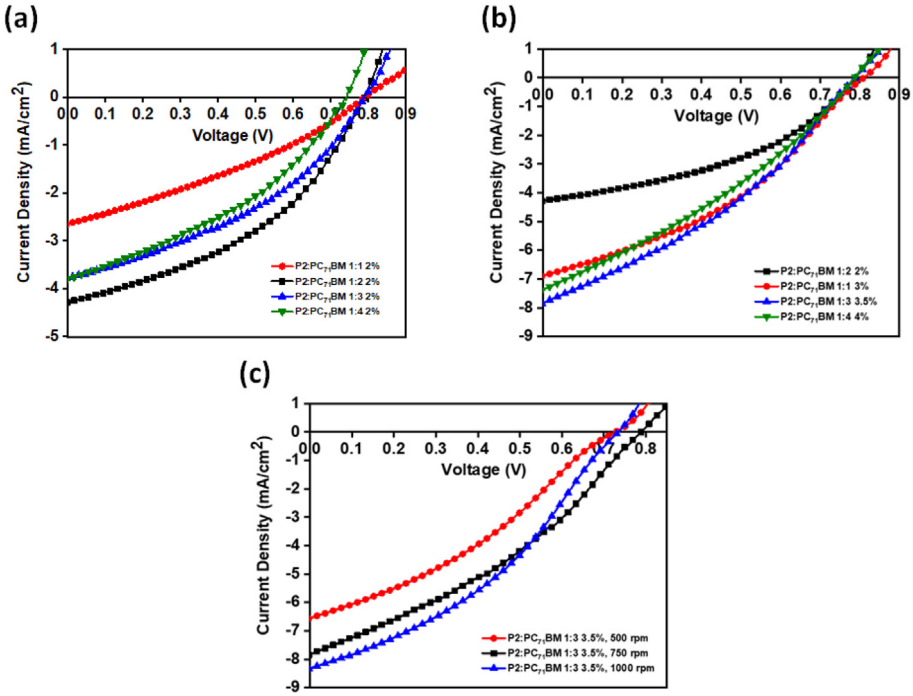

Fig. 9. Current density–voltage curve of P2 for study of a) blend ratio b) concentration c) thickness.

The effect of DPE on the photovoltaic performance of P2 and P4 was tested also. However, the DPE treatment resulted in significant decrease in the photovoltaic performance of P2 and P4 based devices.

According to the photovoltaic studies, the best photovoltaic performance belongs to P1 based devices. The computational studies showed that high hole mobility, polarizability and hyperpolarizability of the P1 exhibits higher dispersion and dipole–dipole intermolecular interactions with the acceptor $PC_{71}BM$. Therefore, all these results support the higher power conversion efficiency obtained from P1 based devices.

3.5. Morphological studies

Morphology of the active layer is quite important for electron-hole couples to reach the interface between donor and acceptor layers at which charge generation occurs [40–42]. TEM images of the best device performance polymer films were investigated to gain insight into the morphology of the active layers based on P1, P2, and P4. In TEM images, the darker places represent PCBM rich areas, and the lighter places represent polymer rich areas (Fig. 11). As seen from the images, P1:$PC_{71}BM$ blend has the most homogenous morphology,

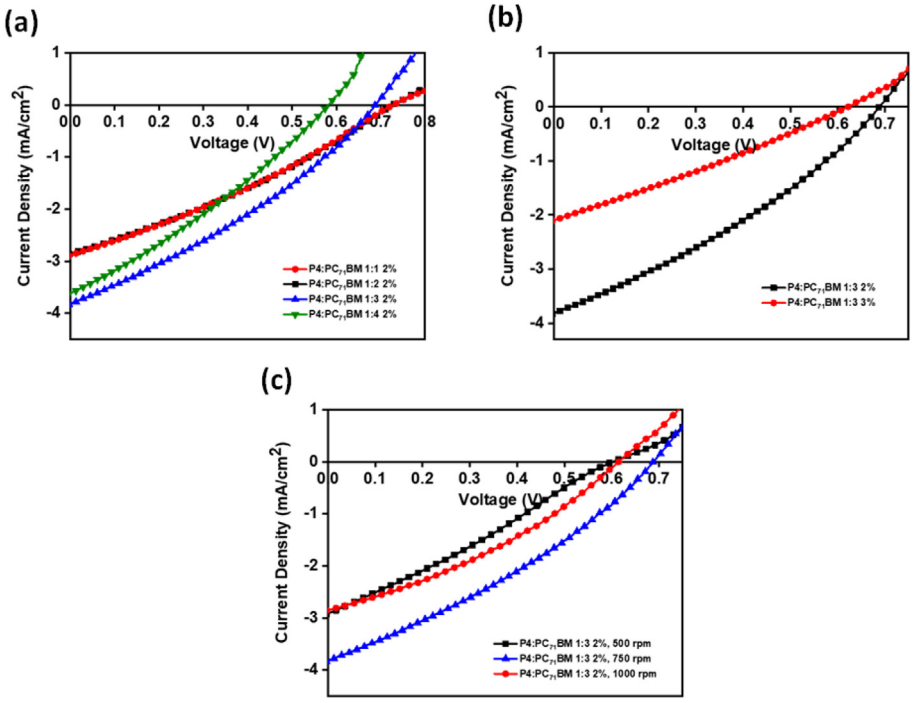

Fig. 10. Current density–voltage curve of P4 for study of a) blend ratio b) concentration c) thickness.

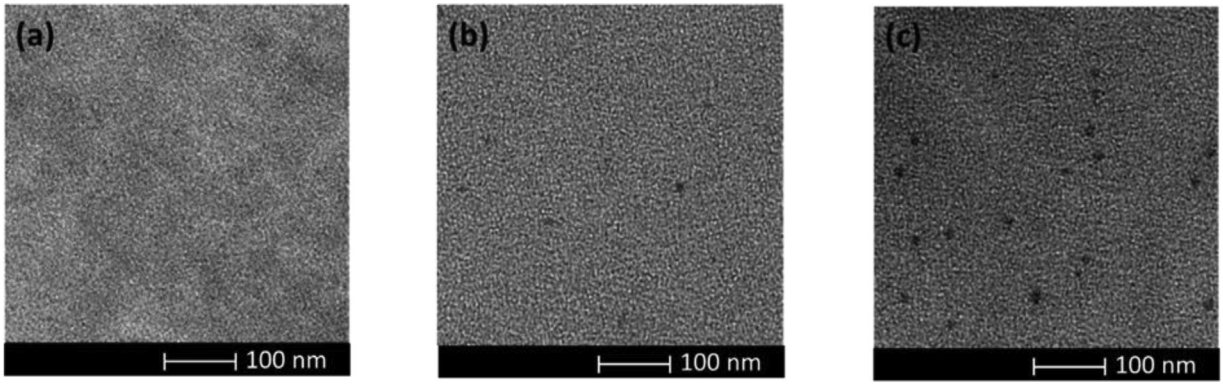

Fig. 11. TEM images of a) P1:$PC_{71}BM$ (1:3 / w:w) blend with 6% DPE at 750 rpm, b) P2:$PC_{71}BM$ (1:2 / w:w) blend, c) P4:$PC_{71}BM$ (1:3 / w:w) blend.

whereas there are some defects on P2:$PC_{71}BM$ and P4:$PC_{71}BM$ blends, which correspond to aggregation of $PC_{71}BM$. The defects lead to lower FF and J_{SC} values [4344]Fig. 11.

Morphology and the chain length of the polymers of the active layer are quite important parameters that determine the performance of the OPV devices. The improved morphology enhances V_{OC}, J_{SC} and FF by providing higher absorption of light, easier exciton dissociation and charge carrier transfer [40,45]. When the TEM images of the devices based on P1, P2, and P4 were compared, P1 based active layer showed uniform morphology without the formation of aggregations. In addition, chain length plays an important role for the OPV parameters. Since higher chain length provides higher intermolecular charge hopping and higher current values [46]. Among the polymers, P1 (M_w: 79kDa, M_n: 55kDa, PDI: 1.43) has the highest chain length in comparison with P2 (Mw: 27kDa, Mn: 16kDa, PDI: 1.66) and P3 (Mw: 13kDa, Mn: 7kDa, PDI: 1.75). Therefore, P1 has the highest OPV performance with improved morphology and largest chain length.

3.6. Charge carrier mobility studies

Charge carrier mobility is one of the key parameters that directly affect the efficiency of organic solar cells. In order to determine the mobility of the copolymers, SCLC model associated with current density–voltage characteristic under dark was utilized and Child's law was applied.

$$\mathrm{JSCL} = \frac{9}{8}\varepsilon o\theta\varepsilon r\mu\frac{V^2}{L^3}$$

Where, ε_o represents free space permittivity, ε_r represents relative permittivity of the material, μ represents charge carrier mobility, L represents active layer thickness, V represents effective voltage, and J_{SCL} represents current [47]. According to the model, the charge mobility of the copolymers was calculated and reported in Table 7. The highest mobility belongs to P1 with 2.38×10^{-4}.

Table 7
Charge mobility of the copolymers.

Polymer: $PC_{71}BM$	M (cm^2/V.s)
P1: $PC_{71}BM$	2.38×10^{-4}
P2: $PC_{71}BM$	1.31×10^{-4}
P4: $PC_{71}BM$	1.10×10^{-4}

4. Computational results

Although all the single chains were predicted to have helical structures in the long range, the diameter of these helices are larger, and chains are relatively more planar for P1 and P2. ESP surfaces mapped on the tetramers showed that electron rich parts represented by red color are concentrated not only on the fluorene donor and bridging units but also on the alkoxy oxygen and fluorine atoms on the acceptor. Electron deficient parts are distributed on the benzothiadiazole acceptor backbone, alkyl side chain of the alkoxy group in acceptor and hydrogen atoms on the donor and bridging unit. The backbones of the chains have a relatively good donor–acceptor distribution along the chain. While P1 shows the highest level of regularity for repeating ESP donor–acceptor pattern, P3 that has lowest planarity, also has the lower regularity for repeating pattern for ESP. HOMO and HOMO-1 orbital surfaces are highly delocalized both on the donors and acceptors. HOMO and HOMO-1 are complementary where HOMO surfaces are mostly on the middle and HOMO-1 surfaces are on the end groups of the tetramer chain. Contrary, LUMO and LUMO + 1 is highly localized on the acceptor and neighboring bridging units (Fig. 12).

Dihedral angles (θ) between donor, acceptor and bridging units are given in Table 8. Two different types of angles were present between acceptors and bridging units due to the -F and alkoxy substitutions at the two sides of the benzothiadiazole acceptor unit. -F substitution did not affect planarity and the angles were below 1 for P1, P2 and P4, which is slightly larger for P3. However, alkoxy substitution changes planarity significantly where dihedral angles are between 10 and 12 for all bridging units. The most important difference in the planarity of the chains is due the dihedral angle between fluorene donor and bridging units. The torsional angles between donor and bridging unit of P3 is 47.30 due to the repulsions between alkyl side chains which significantly reduce physical and electronic properties. P1, P2 and P4 have 28-30 angle between donor and acceptor units. The planarity of P1, P2 and P4 have close values where all of them presented a helical structure in the long range, with higher helical diameter and increased linearity for P1. Close values were determined by three copolymers other than P3, for the VIP, AIP, VEA and AEA values. P1 and P2 have relatively lower positive ionization potential and more negative electron affinity, that are preferred electronic properties for a successful donor–acceptor chain. Band gaps also have close values for P1, P2 and P4, with the exception of nonplanar P3, where the calculated values are in good agreement with experimental values with their optical band gaps values below 2 eV. The difference in the experimental and computational values may be due to the limited chain length in calculations as well as interchain interactions that are not

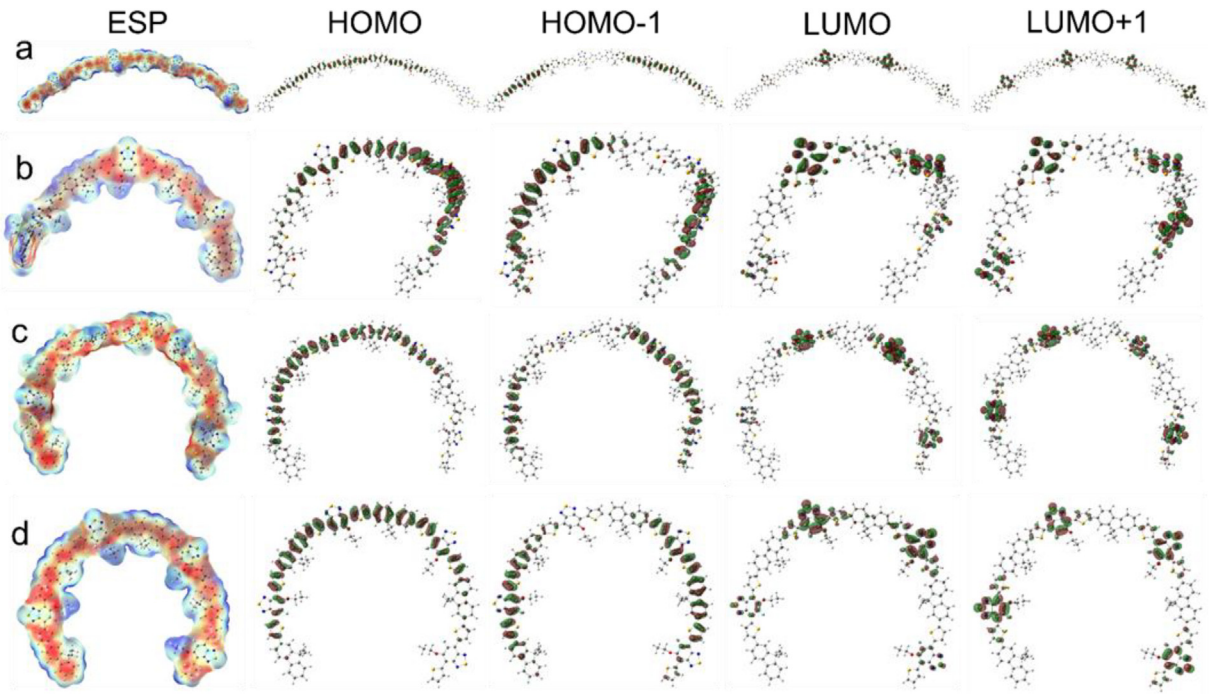

Fig. 12. Electrostatic potential surface (ESP) and frontier orbital surfaces (HOMO, HOMO-1, LUMO, LUMO + 1) for the a) P1, b) P2, c) P3, d) P4 copolymers.

Table 8
Results of the DFT calculations for the electronic and structural properties of P1-P4. (All energies are in eV).

	Θ A-B	θ D-B	HOMO	LUMO	E_g	E_g^{op}	VIP	AIP	VEA	AEA	λ_{reorg}	μ	α	β	δ_A	δ_D	δ_B
P1	0.16\10.83	29.88	−5.10	−2.95	2.15	1.84	5.52	5.48	−2.51	−2.54	0.08	1.84	889.83	29617.20	−0.14	0.67	−0.26
P2	0.37\11.24	29.69	−5.12	−2.90	2.21	1.88	5.60	5.40	−2.41	−2.60	0.11	1.41	677.02	19878.72	−0.22	0.54	−0.18
P3	3.55\10.25	47.30	−5.18	−2.76	2.42	2.11	5.66	5.61	−2.25	−2.29	0.10	1.89	687.79	9565.84	−0.46	0.65	−0.11
P4	0.35\11.60	28.47	−5.12	−2.88	2.24	1.90	5.63	5.57	−2.37	−2.41	0.11	1.38	640.79	17309.49	−0.48	0.54	−0.03

covered in the theoretical calculations. Higher planarity of the chains that leads to the better interchain packing resulted in the lower band compared to the single chain calculations and the most red-shifted neutral state absorption in the experiments. λ_{reorg} value (which are inversely proportional with the mobility) is slightly lower for P1 leading to the higher hole mobility. Dipole moment (μ), polarizability (α) and hyperpolarizability (β) values are also given in Table 8. Significantly higher values of α and β were determined for P1 compared to other copolymers. There is a relation between molecular hyperpolarizability, β, and the bond-length alternation in conjugated chains where β increases with increasing electron delocalization and decreasing bond length alternation [48]. β values have the order of P1 > P2 > P4 > P3 that agrees with the experimental results. Higher polarizability and hyperpolarizability values for P1 also indicated the stronger dispersion and dipole–dipole intermolecular interactions with other species such as $PC_{71}BM$. Finally, atomic charges by ESP fitting on the donor, acceptor and bridging unit for the two repeating units in the middle of tetramers were calculated by neglecting end groups to avoid end group effect. All copolymers have electron transfer from donor to acceptor according to these atomic charges. There are significant positive charges formed on the fluorene donor that demonstrate its efficiency as a donor unit. Bridging units have negative charges that agree with the LUMO levels which are observed to be extended from acceptor to the bridges.

5. Conclusion:

In this work, four novel benzothiadiazole comprising polymers were synthesized via Pd catalyzed Suzuki polycondensation reaction. Electrochemical works revealed that the lowest oxidation potential belongs to P1, which contains electron-rich thienothiophene. In addition, all polymers have a suitable band gap and HOMO-LUMO energy levels for photovoltaic applications. The HOMO energy levels are −5.70 eV, −5.87 eV, −5.90 eV, −5.89 eV and the LUMO energy levels are −3.85 eV, −4.06 eV, −3.80 eV, 3.71 eV for P1, P2, P3, P4, respectively. According to spectroelectrochemical works, the onset of neutral absorption maxima wavelengths was reported as 670 nm, 685 nm, 636 nm, 717 nm, and optical band gaps are evaluated as 1.85 eV, 1.81 eV, 1.95 eV, and 1.73 eV, respectively. These low band gap values showed that all polymers are suitable to construct organic solar cells [49]. Therefore, BHJ solar cell device architectures were constructed for P1, P2, and P4. The power conversion efficiencies were reported as 4.25%, 2.26%, and 0.84% respectively under illumination (AM 1.5 G, 100 mW cm^2). All polymers showed the multi-electrochromic property in their neutral, and doped states. Therefore, they are also promising for electrochromic device construction. Finally, computational studies were conducted to explain origins of the observed experimental performances of polymers at molecular and electronic scale. According to electrostatic potential surface map, HOMO and LUMO energy levels of the copolymers are perfectly distributed along the molecule and donors are electron rich and acceptors are electron poor. In addition, DFT results revealed higher OPV performance of the P1 as the greater charge carrier mobility and better intermolecular interaction with the acceptor in the active layer.

Declaration of Competing Interest

The authors declare that they have no known competing financial interests or personal relationships that could have appeared to influence the work reported in this paper.

Acknowledgements

The authors are thankful to METU Central Lab for HRMS results of the monomers. Erol Yıldırım gratefully acknowledges support from 2232 International Fellowship for Outstanding Researchers Program of TÜBİTAK (Project No: 118C251).

References:

[1] T. Li, W. Zhu, R. Shen, H.-Y. Wang, W. Chen, S.-J. Hao, Y. Li, Z.-G. Gu, Z. Li, Three-dimensional conductive porous organic polymers based on tetrahedral polythiophene for high-performance supercapacitors, New J. Chem. 42 (8) (2018) 6247–6255, https://doi.org/10.1039/C8NJ00667A.

[2] E. Isik, S. Goker, G. Hizalan, S.O. Hacioglu, L. Toppare, Random copolymers of 1,2,3-benzotriazole and alkoxy-modified naptho[2,3-b:3,4-b′]dithiophene: Syntheses, characterization and optoelectronic properties, J. Electroanal. Chem. 786 (2017) 50–57, https://doi.org/10.1016/j.jelechem.2017.01.010.

[3] E. Buber, M. Kesik, S. Soylemez, L. Toppare, A bio-sensing platform utilizing a conjugated polymer, carbon nanotubes and PAMAM combination, J. Electroanal. Chem. 799 (2017) 370–376, https://doi.org/10.1016/j.jelechem.2017.06.043.

[4] D.H. Apaydin, H. Akpinar, M. Sendur, L. Toppare, Electrochromism in multichromic conjugated polymers: Thiophene and azobenzene derivatives on the main chain, J. Electroanal. Chem. 665 (2012) 52–57, https://doi.org/10.1016/j.jelechem.2011.11.016.

[5] T. Sudyoadsuk, P. Chasing, C. Chaiwai, T. Chawanpunyawat, T. Kaewpuang, T. Manyum, S. Namuangruk, V. Promarak, Highly fluorescent solid-state benzothiadiazole derivatives as saturated red emitters for efficient solution-processed non-doped electroluminescent devices, J. Mater. Chem. C. 8 (30) (2020) 10464–10473, https://doi.org/10.1039/D0TC02131H.

[6] B. Zhang, X. Hu, M. Wang, H. Xiao, X. Gong, W. Yang, Y. Cao, Highly efficient polymer solar cells based on poly(carbazole-alt-thiophene- benzofurazan), New J. Chem. 36 (2012) 2042–2047, https://doi.org/10.1039/c2nj40309a.

[7] M. Barłóg, X. Zhang, I. Kulai, D.S. Yang, D.N. Sredojevic, A. Sil, X. Ji, K.S.M. Salih, H.S. Bazzi, H. Bronstein, L. Fang, J. Kim, T.J. Marks, X. Guo, M. Al-Hashimi, Indacenodithiazole-Ladder-Type Bridged Di(thiophene)-Difluoro-Benzothiadiazole-Conjugated Copolymers as Ambipolar Organic Field-Effect Transistors, Chem. Mater. 31 (22) (2019) 9488–9496, https://doi.org/10.1021/acs.chemmater.9b0352510.1021/acs.chemmater.9b03525.s001.

[8] D.i. Zhang, M. Wang, X. Liu, J. Zhao, Synthesis and characterization of donor-acceptor type conducting polymers containing benzotriazole acceptor and benzodithiophene donor or: S -indacenodithiophene donor, RSC Adv. 6 (96) (2016) 94014–94023, https://doi.org/10.1039/C6RA20480E.

[9] D. Liu, L. Sun, Z. Du, M. Xiao, C. Gu, T. Wang, S. Wen, M. Sun, R. Yang, Benzothiadiazole-an excellent acceptor for indacenodithiophene based polymer solar cells, RSC Adv. 4 (71) (2014) 37934–37940, https://doi.org/10.1039/C4RA06967F.

[10] R. Raja, S. Luo, C.Y. Hsiow, S.P. Rwei, L. Wang, Novel two-dimensional conjugated polymer containing fluorinated bithiophene as donor and benzoselenodiazole as acceptor units with vinyl-terthiophene pendants for polymer photovoltaic cells, Polymers (Basel). 9 (2017) 272, https://doi.org/10.3390/polym9070272.

[11] R. Kroon, R. Gehlhaar, T.T. Steckler, P. Henriksson, C. Müller, J. Bergqvist, A. Hadipour, P. Heremans, M.R. Andersson, New quinoxaline and pyridopyrazine-based polymers for solution-processable photovoltaics, Sol. Energy Mater. Sol. Cells. 105 (2012) 280–286, https://doi.org/10.1016/j.solmat.2012.06.029.

[12] R. Stalder, J. Mei, J.R. Reynolds, Isoindigo-based donor-acceptor conjugated polymers, Macromolecules. 43 (20) (2010) 8348–8352, https://doi.org/10.1021/ma1018445.

[13] T. Nakamura, Y. Ishikura, N. Arakawa, M. Hori, M. Satou, M. Endo, H. Masui, S. Fuse, T. Takahashi, Y. Murata, R. Murdey, A. Wakamiya, Donor-acceptor polymers containing thiazole-fused benzothiadiazole acceptor units for organic solar cells, RSC Adv. 9 (13) (2019) 7107–7114, https://doi.org/10.1039/C9RA00229D.

[14] L. Xiao, B. Liu, X. Chen, Y. Li, W. Tang, Y. Zou, Fluorine substituted benzothiazole-based low bandgap polymers for photovoltaic applications, RSC Adv. 3 (2013) 11869–11876, https://doi.org/10.1039/c3ra41140k.

[15] N. Wang, Z. Chen, W. Wei, Z. Jiang, Fluorinated benzothiadiazole-based conjugated polymers for high-performance polymer solar cells without any processing additives or post-treatments, J. Am. Chem. Soc. 135 (45) (2013) 17060–17068, https://doi.org/10.1021/ja409881g.

[16] A. Slodek, M. Matussek, M. Filapek, G. Szafraniec-Gorol, A. Szlapa, I. Grudzka-Flak, M. Szczurek, J.G. Malecki, A. Maron, E. Schab-Balcerzak, E.M. Nowak, J. Sanetra, M. Olejnik, W. Danikiewicz, S. Krompiec, Small Donor-Acceptor Molecules Based on a Quinoline-Fluorene System with Promising Photovoltaic Properties, European J. Org. Chem. 2016 (14) (2016) 2500–2508, https://doi.org/10.1002/ejoc.201600318.

[17] X. Wang, Y. Sun, S. Chen, X. Guo, M. Zhang, X. Li, Y. Li, H. Wang, Effects of π-conjugated bridges on photovoltaic properties of donor-π-acceptor conjugated copolymers, Macromolecules. 45 (3) (2012) 1208–1216, https://doi.org/10.1021/ma202656b.

[18] J. Liu, J. Ren, S. Zhang, J. Hou, Effects on the photovoltaic properties of copolymers with five-membered chalcogen-π-heterocycle bridges, Polym. Chem. 11 (31) (2020) 5019–5028, https://doi.org/10.1039/D0PY00752H.

[19] Y. Zhao, L.i. Zhang, S. Liu, C. Yang, J. Yi, C. Yang, Thieno[3,2-b]thiophene-Bridged Conjugated Polymers Based on Dithieno[3,2-b:2′,3′-d]silole and Thieno[3,4-c]pyrrole-4,6-dione for Polymer Solar Cells: Influence of Side Chains on Optoelectronic Properties, Macromol. Chem. Phys. 219 (24) (2018) 1800297, https://doi.org/10.1002/macp.201800297.

[20] C.Z. Karaman, S. Göker, S.O. Hacioğlu, T. Hacıefendioğlu, E. Yıldırım, L. Toppare, Altering Electronic and Optical Properties of Novel Benzothiadiazole Comprising

Homopolymers via π Bridges, J. Electrochem. Soc. 168 (3) (2021) 036514, https://doi.org/10.1149/1945-7111/abedc5.
[21] P.J. Stephens, F.J. Devlin, C.F. Chabalowski, M.J. Frisch, LETTERS Ab Initio Calculation of Vibrational Absorption and Circular Dichroism Spectra Using Density Functional Force Fields, Phys. Chem. & copy. 98 (1994) (accessed May 11, 2021) https://pubs.acs.org/sharingguidelines.
[22] A.D. Becke, Densityâfunctional thermochemistry. I. The effect of the exchangeâonly gradient correction, J. Chem. Phys. 96 (1992) 2155–2160, https://doi.org/10.1063/1.462066.
[23] C. Lee, W. Yang, R.G. Parr, Development of the Colle-Salvetti correlation-energy formula into a functional of the electron density, Phys. Rev. B. 37 (2) (1988) 785–789, https://doi.org/10.1103/PhysRevB.37.785.
[24] J. R. Cheeseman, G. Scalmani, V. Barone, G. A. Petersson, H. Nakatsuji, X. Li, M. Caricato, A. Marenich, J. Bloino, B. G. Janesko, R. Gomperts, B. Mennucci, H. P. Hratchian, J. V. Ortiz, A. F. Izmaylov, J. L. Sonnenberg, D. Williams-Young, F. Ding, F. Lipparini, F. Egidi, J. Goings, B. Peng, A. Petrone, T. Henderson, D. Ranasinghe, V. G. Zakrzewski, J. Gao, NRega, G. Zheng, W. Liang, MHada, M. Ehara, K. Toyota, R. Fukuda, J. Hasegawa, M. Ishida, T. Nakajima, Y. Honda, O. Kitao, H. Nakai, T. Vreven, K. Throssell Jr., J. A. Montgomery, J. E. Peralta, F. Ogliaro, M. Bearpark, J. J. Heyd, E. Brothers, K. N. Kudin, V. N. Staroverov, T. Keith, R. Kobayashi, J. Normand, K. Raghavachari, A. Rendell, J. C. Burant, S. S. Iyengar, J. Tomasi, M. Cossi, J. M. Millam, M. Klene, C. Adamo, R. Cammi, J. W. Ochterski, R. L. Martin, K. Morokuma, O. Farkas, J. B. Foresman, D. J. Fox, Gaussian 09, Gaussian, Inc., Wallingford CT 2009.
[25] H.T. Turan, O. Kucur, B. Kahraman, S. Salman, V. Aviyente, Design of donor-acceptor copolymers for organic photovoltaic materials: A computational study, Phys. Chem. Chem. Phys. 20 (5) (2018) 3581–3591, https://doi.org/10.1039/C7CP08176F.
[26] E.A. Alkan, S. Goker, H. Sarigul, E. Yıldırım, Y.A. Udum, L. Toppare, The impact of [1,2,5]chalcogenazolo[3,4-f]-benzo[1,2,3]triazole structure on the optoelectronic properties of conjugated polymers, J. Polym. Sci. 58 (2020) 956–968, https://doi.org/10.1002/pol.20190275.
[27] S.C. Cevher, G. Hizalan, E. Alemdar Yilmaz, D. Cevher, Y. Udum Arslan, L. Toppare, E. Yıldırım, A. Cirpan, A comprehensive study: Theoretical and experimental investigation of heteroatom and substituent effects on frontier orbitals and polymer solar cell performances, J. Polym. Sci. 58 (19) (2020) 2792–2806, https://doi.org/10.1002/pola.v58.1910.1002/pol.20200513.
[28] M. Yasa, A. Deniz, M. Forough, E. Yildirim, O. Persil Cetinkol, Y.A. Udum, L. Toppare, Construction of amperometric biosensor modified with conducting polymer/carbon dots for the analysis of catechol, J. Polym. Sci. 58 (23) (2020) 3336–3348, https://doi.org/10.1002/pola.v58.2310.1002/pol.20200647.
[29] J.L. Brédas, D. Beljonne, V. Coropceanu, J. Cornil, Charge-transfer and energy-transfer processes in π-conjugated oligomers and polymers: A molecular picture, Chem. Rev. 104 (2004) 4971–5003, https://doi.org/10.1021/cr040084k.
[30] B.H. Besler, K.M. Merz, P.A. Kollman, Atomic charges derived from semiempirical methods, J. Comput. Chem. 11 (4) (1990) 431–439, https://doi.org/10.1002/(ISSN)1096-987X10.1002/jcc.v11:410.1002/jcc.540110404.
[31] D. Baran, A. Balan, S. Celebi, B. Meana Esteban, H. Neugebauer, N.S. Sariciftci, L. Toppare, Processable multipurpose conjugated polymer for electrochromic and photovoltaic applications, Chem. Mater. 22 (9) (2010) 2978–2987, https://doi.org/10.1021/cm100372t.
[32] R. Ma, J. Yu, T. Liu, G. Zhang, Y. Xiao, Z. Luo, G. Chai, Y. Chen, Q. Fan, W. Su, G. Li, E. Wang, X. Lu, F. Gao, B. Tang, H. Yan, All-polymer solar cells with over 16% efficiency and enhanced stability enabled by compatible solvent and polymer additives, Aggregate. (2021), https://doi.org/10.1002/agt2.58 e58.
[33] R. Ma, Y. Chen, T. Liu, Y. Xiao, Z. Luo, M. Zhang, S. Luo, X. Lu, G. Zhang, Y. Li, H.e. Yan, K. Chen, Improving the performance of near infrared binary polymer solar cells by adding a second non-fullerene intermediate band-gap acceptor, J. Mater. Chem. C. 8 (3) (2020) 909–915, https://doi.org/10.1039/C9TC06362E.
[34] R. Ma, G. Li, D. Li, T. Liu, Z. Luo, G. Zhang, M. Zhang, Z. Wang, S. Luo, T. Yang, F. Liu, H.e. Yan, B.o. Tang, Understanding the Effect of End Group Halogenation in Tuning Miscibility and Morphology of High-Performance Small Molecular Acceptors, Sol. RRL. 4 (9) (2020) 2000250, https://doi.org/10.1002/solr.v4.910.1002/solr.202000250.
[35] N.K. Elumalai, A. Uddin, Open circuit voltage of organic solar cells: An in-depth review, Energy Environ. Sci. 9 (2) (2016) 391–410, https://doi.org/10.1039/C5EE02871J.
[36] H. Unay, N.A. Unlu, G. Hizalan, S.O. Hacioglu, D.E. Yildiz, L. Toppare, A. Cirpan, Benzotriazole and benzodithiophene containing medium band gap polymer for bulk heterojunction polymer solar cell applications, J. Polym. Sci. Part A Polym. Chem. 53 (4) (2015) 528–535, https://doi.org/10.1002/pola.27467.
[37] T.H. Lee, S.Y. Park, B. Walker, S.-J. Ko, J. Heo, H.Y. Woo, H. Choi, J.Y. Kim, A universal processing additive for high-performance polymer solar cells, RSC Adv. 7 (13) (2017) 7476–7482, https://doi.org/10.1039/C6RA27944A.
[38] R.T. Ginting, C.C. Yap, M. Yahaya, V. Fauzia, M.M. Salleh, Active layer spin coating speed dependence of inverted organic solar cell based on Eosin-Y-coated ZnO nanorod arrays, in, J. Phys. Conf. Ser., Institute of Physics Publishing 431 (2013) 012016, https://doi.org/10.1088/1742-6596/431/1/012016.
[39] R. Ma, Y. Tao, Y. Chen, T. Liu, Z. Luo, Y. Guo, Y. Xiao, J. Fang, G. Zhang, X. Li, X. Guo, Y. Yi, M. Zhang, X. Lu, Y. Li, H.e. Yan, Achieving 16.68% efficiency ternary as-cast organic solar cells, Sci. China Chem. 64 (4) (2021) 581–589, https://doi.org/10.1007/s11426-020-9912-0.
[40] R. Ma, T. Liu, Z. Luo, K.e. Gao, K. Chen, G. Zhang, W. Gao, Y. Xiao, T.-K. Lau, Q. Fan, Y. Chen, L.-K. Ma, H. Sun, G. Cai, T. Yang, X. Lu, E. Wang, C. Yang, A.-Y. Jen, H.e. Yan, Adding a Third Component with Reduced Miscibility and Higher LUMO Level Enables Efficient Ternary Organic Solar Cells, ACS Energy Lett. 5 (8) (2020) 2711–2720, https://doi.org/10.1021/acsenergylett.0c0136410.1021/acsenergylett.0c01364.s001.
[41] T. Liu, T. Yang, R. Ma, L. Zhan, Z. Luo, G. Zhang, Y. Li, K.e. Gao, Y. Xiao, J. Yu, X. Zou, H. Sun, M. Zhang, T.A. Dela Peña, Z. Xing, H. Liu, X. Li, G. Li, J. Huang, C. Duan, K.S. Wong, X. Lu, X. Guo, F. Gao, H. Chen, F. Huang, Y. Li, Y. Li, Y. Cao, B.o. Tang, H.e. Yan, 16% efficiency all-polymer organic solar cells enabled by a finely tuned morphology via the design of ternary blend, Joule. 5 (4) (2021) 914–930, https://doi.org/10.1016/j.joule.2021.02.002.
[42] K. Goksu, G. Hizalan, Y.A. Udum, S.O. Hacioglu, S.C. Cevher, Akrema, L. Toppare, A. Cirpan, Syntheses and Characterization of Benzotriazole, Thienopyrroledione, and Benzodithiophene Containing Conjugated Random Terpolymers for Organic Solar Cells, J. Electrochem. Soc. 166 (15) (2019) H849–H859, https://doi.org/10.1149/2.1161915jes.
[43] A. Cetin, C. Istanbulluoglu, S.O. Hacioglu, S.C. Cevher, L. Toppare, A. Cirpan, Synthesis of bistriphenylamine- and benzodithiophene-based random conjugated polymers for organic photovoltaic applications, J. Polym. Sci. Part A Polym. Chem. 55 (22) (2017) 3705–3715, https://doi.org/10.1002/pola.v55.2210.1002/pola.28752.
[44] T. Liu, R. Ma, Z. Luo, Y. Guo, G. Zhang, Y. Xiao, T. Yang, Y. Chen, G. Li, Y. Yi, X. Lu, H. Yan, B. Tang, Concurrent improvement in: J SCand v OCin high-efficiency ternary organic solar cells enabled by a red-absorbing small-molecule acceptor with a high LUMO level, Energy Environ. Sci. 13 (2020) 2115–2123. https://doi.org/10.1039/d0ee00662a.
[45] K. Hussain, W. Kaiser, A. Gagliardi, Effect of Polymer Morphology on Dilute Donor Organic Solar Cells, J. Phys. Chem. C. 124 (6) (2020) 3517–3528, https://doi.org/10.1021/acs.jpcc.9b1160910.1021/acs.jpcc.9b11609.s001.
[46] G. Li, X. Gong, J. Zhang, Y. Liu, S. Feng, C. Li, Z. Bo, 4-Alkyl-3,5-difluorophenyl-Substituted Benzodithiophene-Based Wide Band Gap Polymers for High-Efficiency Polymer Solar Cells, ACS Appl. Mater. Interfaces. 8 (6) (2016) 3686–3692, https://doi.org/10.1021/acsami.5b0876910.1021/acsami.5b08769.s001.
[47] S.O. Hacioglu, N.A. Unlu, E. Aktas, G. Hizalan, E.D. Yildiz, A. Cirpan, L. Toppare, A triazoloquinoxaline and benzodithiophene bearing low band gap copolymer for electrochromic and organic photovoltaic applications, Synth. Met. 228 (2017) 111–119, https://doi.org/10.1016/j.synthmet.2017.04.017.
[48] S.M. Risser, N. Beratan,', S.R. Marder, Structure-Function Relationships for 0, the First Molecular Hyperpolarizability, 1993. https://pubs.acs.org/sharingguidelines (accessed May 11, 2021).
[49] R. Ma, M. Zeng, Y. Li, T. Liu, Z. Luo, Y.e. Xu, P. Li, N. Zheng, J. Li, Y. Li, R. Chen, J. Hou, F. Huang, H.e. Yan, Rational Anode Engineering Enables Progresses for Different Types of Organic Solar Cells, Adv. Energy Mater. 11 (23) (2021) 2100492, https://doi.org/10.1002/aenm.v11.2310.1002/aenm.202100492.